PHYSICAL REVIEW B VOLUME 18, NUMBER 9 1 NOVEMBER 1978

Insulating phase of V_2O_3: An attempt at a realistic calculation

C. Castellani,* C. R. Natoli,† and J. Ranninger
Groupe des Transitions de Phases, Centre National de la Recherche Scientifique, Boîte Postale 166, 38042 Grenoble Cedex, France

(Received 14 June 1977)

The problem of the highly correlated electron gas V_2O_3 consisting of a filled a_{1g} and a quarterly full e_g band is treated on the basis of a Hartree-Fock calculation with spin and orbit unrestriction. The values of the effective hopping integrals which include covalency effects (due to the overlap of the $2p_\pi$ orbitals of the oxygens with the $3d$ wave functions of the vanadium atoms) are assessed on the bases of available band-structure calculations and experimental results measuring covalency contributions. For reasonable values of the Hubbard parameters $U_{mm} \simeq 2$ eV, $U_{mn} \simeq 1.6$ eV, and $J_{mn} \simeq 0.2$ eV [the interatomic Coulomb repulsion of electrons on the same orbit (m,m) on different orbits (m,n) and the exchange integral J_{mn}] it is found that the observed spin structure of V_2O_3 together with an antiferromagnetic orbital order gives the lowest Hartree-Fock ground-state energy amongst a large class of solutions which we considered and shows a gap in the density of states of the order of 0.2–0.3 eV. Since this gap appears already in the trigonal phase, we feel confident that the monoclinic distortion in the low-temperature phase is of magnetostrictive origin and not a primary cause of the metal-insulator transition. The peculiar value of $1.2\mu_B$ per V atom as observed by neutron scattering is interpreted as a strongly covalency-enhanced moment on the V atom. The atomic limit value of $1\mu_B$ due to one magnetic e_g electron per V atom is reduced to $\simeq 0.75\mu_B$ in an itinerant picture. The covalency mechanism providing the extra $0.4\mu_B$ is known as back-bonding effect and leads at the same time to a negative spin density on the oxygen ions which are therefore no longer diamagnetic. Negative ^{17}O NMR shift in the insulating antiferromagnetic phase should be able to verify this conjecture.

I. INTRODUCTION

The understanding of the two transitions observed in V_2O_3 around 150 and 500 °K requires as a first step a proper description of the interelectronic correlations both in the insulating phase at low temperature and in the metallic phase between 150 and 300 °K. Indeed, this has been the aim of the preceding paper[1] (hereafter referred to as I) where we have studied the atomic limit of the model Hamiltonian appropriate to V_2O_3 with the intuitive conviction that the correlations found there would persist in the physical region $W/U \sim 1$ at least at the short-range level within the metallic phase, and as long-range order in the insulating phase. The need to corroborate this conviction has motivated the work reported in this, the second paper of a series, where we attempt a "realistic" calculation of the metallic and insulating phase. We think, in fact, that a good agreement between theoretical calculations and experimental evidence in this last phase is essential for the understanding of electron correlations in V_2O_3. The word "realistic" is used to indicate two levels of approximation to the physical reality. On one hand it means that we introduce into the problem the complex band structure of the magnetic $3d$ electrons in the t_{2g} subband and take into proper account the role of the "diamagnetic" ligands; on the other hand it indicates that the kind of mathematical approximation used to solve the problem (namely the unrestricted Hartree-Fock approximation) is one which approximates the exact solution in a satisfactory way. The first goal is achieved by adopting the point of view indicated by Anderson[2] in discussing superexchange. It consists in describing the $3d$ antibonding electrons of the cations as being in Wannier states of the form

$$\psi_i(\vec{x}) = (1/N_\pi^{1/2})[\phi^{3d}{}_i(\vec{x}) - \lambda_\pi \chi^\pi{}_i(\vec{x})] , \tag{1.1}$$

where $\phi_i^{3d}(\vec{x})$ is the $3d$ normalized wave function of t_{2g} character for the electrons at the site i, and $\chi_i^\pi(\vec{x})$ is the corresponding (same symmetry) normalized wave function of the cluster of six oxygen atoms surrounding the cation site (their explicit expression will be given in Sec. II).

The constant N_π is the proper normalization factor given by

$$N_\pi = 1 - 2\lambda_\pi S_\pi(\phi_i^{3d}, \chi_i^\pi) + \lambda_\pi^2 , \tag{1.2}$$

where $S_\pi(\phi_i^{3d}, \chi_i^\pi)$ is the overlap integral of π type between the two functions ϕ_i^{3d} and $\chi_{i'}^\pi$, and λ_π is the antibonding covalency mixture parameter obtainable from NMR measurements at the ligand sites.

Actually a more correct form of Wannier function relative to a site i, is one which is normalized to the ones centered at the neighboring sites and is given by

$$w_i(\vec{x}) = \psi_i(\vec{x}) - \tfrac{1}{2} \sum_j S_{ij}\psi_j(\vec{x}) \tag{1.3}$$

to first order in the overlap integral $S_{ij} = \langle \psi_i | \psi_j \rangle$.

Using these Wannier type of functions one finds, as will be shown in Sec. II, that the effective transfer integral between two $3d$ electrons sitting at sites i and j is

$$\langle w_i(\vec{x}) | H_0 | w_j(\vec{x}) \rangle = [\lambda_\pi^2 (E_{3d} - E_{2p_\pi}) \langle \chi_i | \chi_j \rangle + \langle \phi_{3d}^i(\vec{x}) | H_0 | \phi_{3d}^j(\vec{x}) \rangle] N_\pi^{-1} , \tag{1.4}$$

where $\Delta E = E_{3d} - E_{2p_\pi}$ is the average energy difference between the energy of the $3d$ antibonding electrons and that of the $2p_\pi$ electrons in the cluster. The quantity $\langle \chi_i | \chi_j \rangle$ is a numerical coefficient easily calculated from the knowledge of the cluster wave functions centered at neighboring cation sites i and j.

Expression (1.4) allows a reasonable estimation of the effective transfer integrals since λ_π is known from NMR measurements at ligand sites. The energy difference $\Delta E = E_{3d} - E_{2p_\pi}$ is obtainable from optical or photoemission spectra.

The quantity $\langle \phi_i^{3d} | H_0 | \phi_j^{3d} \rangle$ can be calculated with a fair degree of accuracy. In the case of the metallic phase of V_2O_3, λ_π^2 turns out to be 0.3 with 50% accuracy[3] and $\Delta E = 4$–5 eV as obtained from photoemission and soft-x-ray absorption and emission spectra,[4] $\langle \phi_i^{3d} | H_0 | \phi_j^{3d} \rangle$ having been calculated by Ashkenazi and Chuchem.[5] Thus a sound basis is provided for a "realistic" description of the $3d$-t_{2g} subband.

Concerning the second point, that is to say a satisfactory approximation to the exact solution of the model Hamiltonian (2.3) in I, we divide *ab initio* the whole lattice into two or more sublattices and use a first-order Green's-functions decoupling scheme which allows for different occupation numbers for various sublattice spin and orbital occupancies according to the instabilities suggested by the atomic limit calculation. Then a self-consistent solution is sought and the ground-state energies of the various sublattices, spin and orbital configurations, are compared. This is clearly equivalent to an investigation in an unrestricted Hartree-Fock approximation of the instability of the high-symmetry phase (the metallic state) against a breakdown of its symmetry. The advantages and disadvantages of the unrestricted Hartree-Fock approximation have been discussed quite at length in the literature (see Weger,[6] and Ashkenazi and Weger,[7] and references therein). We would just like to point out two aspects of this approximate method of calculation which are relevant for our considerations: First of all, the accuracy of this procedure was tested for the exact result of Lieb and Wu[8] for the one-dimensional nondegenerate case by Langer *et al.*[9] These authors "were pleased to find satisfactory agreement at all values of the ratio U/W, becoming almost exact agreement in the weak coupling limit ($U/W < \frac{1}{3}$)." In more quantitative terms, the discrepancy was found to be of the order of 100% in the worst case ($U/W \sim 1$). From our part we might further comment that the one-dimensional model is the worst case with which to compare the HF procedure due to the limited number of nearest neighbors of each site z ($=2$ in this model). In fact, we expect the corrections to the HF ground-state energy to go like $1/z$. In three dimensions with an increased number of neighbors, the approximation is expected to be better. In particular in the case of V_2O_3, the correlations between vertical pairs will be treated to a satisfactory degree of accuracy since there are twelve neighboring pairs to a given one which interact with about the same strength. However the correlations inside the pairs, where the transfer integrals of the electrons from one site to the other one are substantially bigger than those between pairs, are expected to be treated to the same degree of approximation as for the unidimensional case.

The second aspect we wanted to emphasize can be best illustrated in the case of a diatomic molecule with one electron per site in a nondegenerate Wannier (atomic) state described by a Hubbard Hamiltonian of the type

$$H = t_0 \sum_\sigma (n_{a\sigma} + n_{b\sigma}) + t \sum_\sigma (c_{a\sigma}^\dagger c_{b\sigma} + c_{b\sigma}^\dagger c_{a\sigma}) + \frac{U}{2} \sum_\sigma (n_{a\sigma} n_{a\, -\sigma} + n_{b\sigma} n_{b\, -\sigma}) , \tag{1.5}$$

where a and b indicate the two sites of the molecule.[10] (As a byproduct, this discussion will provide us with more insight into the interelectronic correlation of a pair in V_2O_3). The exact ground-state wave function Ψ and the corresponding energy E_G are easily found to be

$$\Psi = \frac{1}{N} \left((c_{a\uparrow}^\dagger c_{b\downarrow}^\dagger - c_{a\downarrow}^\dagger c_{b\uparrow}^\dagger) |0\rangle + \frac{U - (U^2 + 16t^2)^{1/2}}{4t} \times (c_{a\uparrow}^\dagger c_{a\downarrow}^\dagger + c_{b\uparrow}^\dagger c_{b\downarrow}^\dagger) |0\rangle \right) , \tag{1.6}$$

$$E_G = 2t_0 + \tfrac{1}{2}[U - (U^2 + 16t^2)^{1/2}] , \tag{1.7}$$

where N is a suitable normalization factor.

A straightforward Green's-function calculation on the lines already indicated, allowing for $\langle n_{a\sigma} \rangle - \langle n_{b\sigma} \rangle = \langle \bar{n}_\sigma \rangle \neq 0$, leads to the following results: The one-particle energies are given by

$$\epsilon_\sigma^{1,2} = \tfrac{1}{2}[U \pm (U^2 \langle \bar{n}_{-\sigma} \rangle^2 + 4t^2)^{1/2}] + t_0 \tag{1.8}$$

and the quantities $\langle \bar{n}_\sigma \rangle$ are obtained from the self-consistent equations

$$\langle n_{a\sigma}\rangle = \tfrac{1}{2}[1 - (U/\Delta_{-\sigma})\langle n_{-\sigma}^-\rangle], \tag{1.9}$$

$$\langle n_{b\sigma}\rangle = \tfrac{1}{2}[1 + (U/\Delta_{-\sigma})\langle n_{-\sigma}^-\rangle], \tag{1.10}$$

leading to the following equation for $\langle n_\sigma^-\rangle$:

$$\langle n_\sigma^-\rangle = -(U/\Delta_{-\sigma})\langle n_{-\sigma}^-\rangle , \tag{1.11}$$

where we have defined $\Delta_\sigma = (U^2\langle n_\sigma^-\rangle^2 + 4t^2)^{1/2}$. Examination of (1.11) shows the following: (a) The "molecular-orbital" solution (MO) $\langle n_\sigma^-\rangle = 0$ is always possible. (b) If $2|t/U| = 2x < 1$ and $U > 0$ a spin-density-wave solution (SDW) becomes possible with

$$\langle n_{a\sigma}\rangle = \tfrac{1}{2}\{1 - 2\sigma[1 - (2x)^2]^{1/2}\}$$

$$= \sin^2\theta\, \delta_{\sigma,1/2} + \cos^2\theta\, \delta_{\sigma,-1/2}, \tag{1.12}$$

$$\langle n_{b\sigma}\rangle = \tfrac{1}{2}\{1 + 2\sigma[1 - (2x)^2]^{1/2}\}$$

$$= \cos^2\theta\, \delta_{\sigma,1/2} + \sin^2\theta\, \delta_{\sigma,-1/2}, \tag{1.13}$$

where $\sin 2\theta = 2x$ and $\sigma = \pm\frac{1}{2}$. (c) If $2x < 1$ and $U < 0$ a charge-density-wave solution (CDW) becomes possible with

$$\langle n_{a\sigma}\rangle = \tfrac{1}{2}\{1 - [1 - (2x)^2]^{1/2}\} = \sin^2\theta, \tag{1.14}$$

$$\langle n_{b\sigma}\rangle = \tfrac{1}{2}\{1 + [1 - (2x)^2]^{1/2}\} = \cos^2\theta . \tag{1.15}$$

The ground-state energy of the molecule in this approximation is easily calculated to be

$$E_G = U - \tfrac{1}{2}(\Delta_\sigma + \Delta_{-\sigma}) - \tfrac{1}{2}U(1 + n_{-\sigma}^- n_\sigma^-) + 2t_0 . \tag{1.16}$$

Hence for the three cases (a), (b), and (c) above, we get

$$\begin{aligned} E_G^{(a)} &= \tfrac{1}{2}U - 2|t| + 2t_0 ,\\ E_G^{(b)} &= -2|t^2/U| + 2t_0 ,\\ E_G^{(c)} &= -(|U| + 2|t^2/U|) + 2t_0 , \end{aligned} \tag{1.17}$$

having used Eq. (1.11).

Inspection of E_G for the three cases shows that the MO solution [case (a)] is stable for $|U/t| \leqslant 2$; the SDW solution [case (b)] is stable for $U/|t| > 2$; and the CDW solution is stable for $U/|t| < -2$. The corresponding ground-state wave functions are easily obtained from the expression of the occupation numbers. The results are (a) MO state:

$$\Psi = (c_{a\uparrow}^\dagger + c_{b\uparrow}^\dagger)(c_{a\downarrow}^\dagger + c_{b\downarrow}^\dagger)|0\rangle ;$$

(b) SDW state:

$$\Psi_1 = \cos\theta\sin\theta(c_{a\uparrow}^\dagger c_{a\downarrow}^\dagger + c_{b\uparrow}^\dagger c_{b\downarrow}^\dagger)|0\rangle$$

$$+ \cos^2\theta\, c_{a\uparrow}^\dagger c_{b\downarrow}^\dagger + \sin^2\theta\, c_{b\uparrow}^\dagger c_{a\downarrow}^\dagger)|0\rangle$$

or

$$\begin{aligned} \psi_2 = {}& \cos\theta\sin\theta(c_{a\uparrow}^\dagger c_{a\downarrow}^\dagger + c_{b\uparrow}^\dagger c_{b\downarrow}^\dagger\rangle|0\rangle \\ &+ (\sin^2\theta\, c_{a\uparrow}^\dagger c_{b\downarrow}^\dagger + \cos^2\theta\, c_{b\uparrow}^\dagger c_{a\downarrow}^\dagger)|0\rangle ; \end{aligned} \tag{1.18}$$

(c) CDW state:

$$\begin{aligned} \psi_1 = {}& (\cos^2\theta\, c_{a\uparrow}^\dagger c_{a\downarrow}^\dagger + \sin^2\theta\, c_{b\uparrow}^\dagger c_{b\downarrow}^\dagger)|0\rangle \\ &+ \sin\theta\cos\theta(c_{a\uparrow}^\dagger c_{b\downarrow}^\dagger + c_{b\uparrow}^\dagger c_{a\downarrow}^\dagger)|0\rangle \end{aligned}$$

or

$$\begin{aligned} \psi_2 = {}& (\sin^2\theta\, c_{a\uparrow}^\dagger c_{a\downarrow}^\dagger + \cos^2\theta\, c_{b\uparrow}^\dagger c_{b\downarrow}^\dagger)|0\rangle \\ &+ \sin\theta\cos\theta(c_{a\uparrow}^\dagger c_{b\downarrow}^\dagger + c_{b\uparrow}^\dagger c_{a\downarrow}^\dagger)|0\rangle \end{aligned}$$

and justifies the denomination given to states. It is to be noticed that the same solution for the wave functions and the ground-state energies could have been obtained from a variational starting from a "generalized" (that is to say unrestricted) trial HF state of the form

$$\begin{aligned} |\phi\rangle = {}& (\cos\theta_1\, c_{a\uparrow}^\dagger + e^{i\chi_1}\sin\theta_1\, c_{b\uparrow}^\dagger) \\ &\times (\cos\theta_2\, c_{a\downarrow}^\dagger + e^{i\chi_2}\sin\theta_2\, c_{b\downarrow}^\dagger)|0\rangle \end{aligned}$$

and minimizing the total energy $(\phi|H|\phi)$ with respect to the parameters $\theta_1, \theta_2, \chi_1, \chi_2$, subject to the restrictions

$$-\tfrac{1}{2}\pi < \theta_i \leqslant \tfrac{1}{2}\pi, \quad 0 \leqslant \chi_i < \pi \quad (i = 1, 2) . \tag{1.19}$$

Obviously the two methods give the same results since it can be shown that they are completely equivalent.

The conclusions to be drawn from the previous considerations are several. First of all, we see from Eqs. (1.17) and (1.7) that the worst approximation occurs for $\frac{1}{2}U/|t| \sim 1$ as was expected. Secondly, even in the region $\frac{1}{2}U/|t| > 1$, the discrepancy between the approximate and the exact ground-state energies is quite appreciable even for $\frac{1}{2}|U/t| \sim 10$ (100%) so that the approximation is not so good in the case of a diatomic molecule which too was to be expected. Perhaps the more disturbing feature of the HF solution is that for the region $\frac{1}{2}|U/t| > 1$, the best approximation to the exact ground-state energy corresponds to a state having an order parameter $\langle n_\sigma^-\rangle = \langle n_{a\sigma}\rangle - \langle n_{b\sigma}\rangle$ different from zero (for example, the staggered magnetization in the SDW state) which does not correspond to the physical reality. In the exact solution indeed the ground state is diamagnetic.

This simple example can serve as a guide to judge an HF solution. In general, if the physical state shows some order parameter (like an antiferromagnetic insulating state or an itinerant antiferromagnetic metallic state) the HF solution provides a rather satisfactory approximation to the ground-state energy and a reliable description of the interelectronic correlations. Unfortunately this description is not so good, for example, in a paramagnetic correlated metal where fluctuations of the physical quantities around their average values are so big that the definition of a steady, average mean field acting on a particle due to the action of the other ones becomes questionable. In such a case, the introduction of a fictitious mean field can help describing the correlation between electrons and, moreover, it might constitute the best way to approximate the unknown ground-state energy.

All this applies to the various phases of V_2O_3. However, even if we can hope to give a reasonable "realistic" calculation only in the low-temperature antiferromagnetic-insulating (AI) phase, nonetheless we shall obtain a great deal of information about the actual correlations between electrons in the metallic phase from a correct interpretation of the AI phase. Consequently, we shall be in a position to speculate about the actual interelectronic correlation in the metallic phase and the actual driving force of the first transition at 150 °K. Also an interpretation of the second transition at 500 °K will be attempted which shall be based on our knowledge of the system around the first transition.

II. CHOICE OF THE WANNIER FUNCTIONS

As already stated in the introduction, a major component of any realistic approach to V_2O_3 must be the correct choice of the Wannier functions. In this section, their explicit expression is derived for the case of the corundum structure, which will allow us to estimate the effective transfer integrals in Eq. (1.4).

Referring to Fig. 1(a), it is a standard result of group theory that the metal-3*d* and ligand-2*p* orbitals in an octahedral complex transforming according to the t_{2g} representation of the O_h group are given by

$$\begin{aligned} &d_{x'z'} \quad \chi^{\pi}_{x'z'} = \tfrac{1}{2}(z'_1 + x'_5 - z'_3 - x'_6)\,, \\ &d_{y'z'} \quad \chi^{\pi}_{y'z'} = \tfrac{1}{2}(z'_2 + y'_5 - z'_4 - y'_6)\,, \qquad (2.1) \\ &d_{x'y'} \quad \chi^{\pi}_{x'y'} = \tfrac{1}{2}(y'_1 + x'_2 - y'_3 - x'_4)\,, \end{aligned}$$

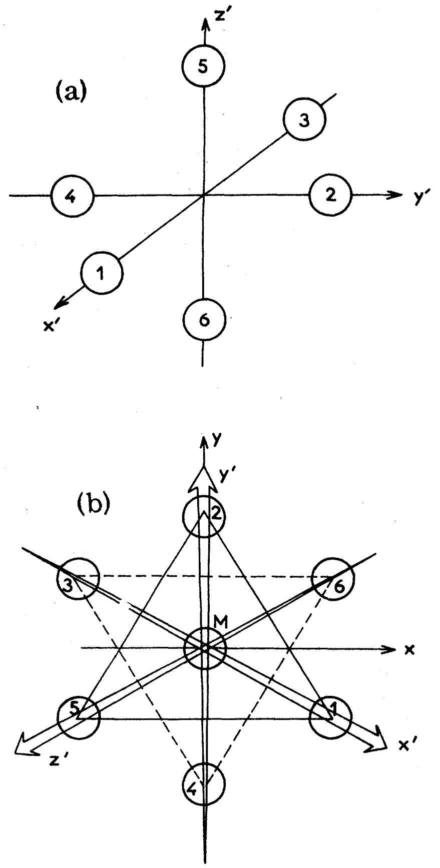

FIG. 1. (a) Octahedral coordination for a central metal ion with primed reference; (b) Same octahedral complex from the trigonal axis chosen as *z* axis in the unprimed reference frame.

where in standard notation $d_{x'z'}$ indicates the normalized 3*d* orbital of $x'z'$ symmetry and z'_1 the normalized $2p_{z'}$ orbital centered at ligand site 1.

Because of the trigonal distortion of the octahedral environment of a cation site in the corundum structure, the appropriate wave functions in the lower D_{3d} symmetry are

$$\begin{aligned} &e_g \begin{cases} (1/\sqrt{2})(d_{x'y'} - d_{y'z'})\,, & (1/\sqrt{2})(\chi^{\pi}_{x'y'} - \chi^{\pi}_{y'z'}) \\ \sqrt{2}/3[d_{x'z'} - \tfrac{1}{2}(d_{x'y'} + d_{y'z'})], & \sqrt{2}/3[\chi^{\pi}_{x'z'} - \tfrac{1}{2}(\chi^{\pi}_{x'y'} + \chi^{\pi}_{y'z'})]\,, \end{cases} \qquad (2.2) \\ &a_{1g}\{(1/\sqrt{3})(d_{x'y'} + d_{x'z'} + d_{y'z'})\,, \quad (1/\sqrt{3})(\chi^{\pi}_{x'y'} + \chi^{\pi}_{x'z'} + \chi^{\pi}_{y'z'})\,, \end{aligned}$$

where it is indicated that the functions of the first two rows transform according to the bidimensional representation e_g while those of the third row transform according to the unidimensional representation a_{1g}.

We shall find it useful for later purposes to take the threefold axis as the axis of quantization and pass from the primed reference frame of Fig. 1(a) to the unprimed reference frame of Fig. 1(b). The transformation relations are as follows:

$$x=(1/\sqrt{2})(x'-z'),$$

$$x'=(1/\sqrt{2})x-(1/\sqrt{6})y+(1/\sqrt{3})z,$$

$$y=-(1/\sqrt{6})(x'-2y'+z'),$$

$$y'=(2/\sqrt{6})y+(1/\sqrt{3})z,$$

$$z=(1/\sqrt{3})(x'+y'+z'),$$

$$z'=-(1/\sqrt{2})x-(1/\sqrt{6})y+(1/\sqrt{3})z. \qquad (2.3)$$

Hence, for the three wave function (1.1) transforming as the e_g and a_{1g} representation we have

$$\psi^1_{\vec{R}}=\frac{1}{N_\pi^{1/2}}\left\{\left(\sqrt{\tfrac{2}{3}}\,d_{xy}+\frac{1}{\sqrt{3}}d_{xz}\right)-\frac{\lambda_\pi}{2\sqrt{2}}\left[\frac{2}{\sqrt{6}}(y_1-y_3-y_5+y_6)+\frac{1}{\sqrt{3}}(z_1-z_3-z_5+z_6)+\sqrt{2}\,(x_2-x_4)\right]\right\},$$

$$\begin{aligned}\psi^2_{\vec{R}_1}=\frac{1}{N_\pi^{1/2}}\Bigg\{\left(\sqrt{\tfrac{2}{3}}\,d_{y^2-x^2}-\frac{1}{\sqrt{3}}d_{yz}\right)-\frac{\lambda_\pi}{\sqrt{6}}\Bigg[&-\frac{1}{\sqrt{2}}(x_1-x_3-x_5+x_6)-\frac{2}{\sqrt{6}}(y_1-y_3+y_5-y_6)\\&+\frac{1}{2\sqrt{3}}(z_1-z_3+z_5-z_6)+\frac{1}{\sqrt{6}}(y_2-y_4)-\frac{1}{\sqrt{3}}(x_2-x_4)\Bigg]\Bigg\}\end{aligned} \qquad (2.4)$$

$$\begin{aligned}\psi^3_{\vec{R}_1}=\frac{1}{N_\pi^{1/2}}\Bigg\{d_{z^2}-\frac{\lambda_\pi}{\sqrt{12}}\Bigg[&\frac{1}{\sqrt{2}}(-x_1+x_3+x_5-x_6)+\frac{1}{\sqrt{6}}(y_1-y_3+y_5-y_6)+\frac{2}{\sqrt{3}}(z_1-z_3+z_5-z_6)\\&-\frac{2}{\sqrt{6}}(y_2-y_4)+\frac{2}{\sqrt{3}}(z_2-z_4)\Bigg]\Bigg\},\end{aligned}$$

where N_π is given by Eq. (1.2). The quantity $S_\pi(\phi^{3d},\chi^\pi)$ appearing in this last equation is easily seen from (2.1) to be given by

$$S_\pi(\phi^{3d},\chi^\pi)=2\langle 3d_\pi|2p_\pi\rangle, \qquad (2.5)$$

where, for instance, $\langle 3d_\pi|2p_\pi\rangle=\langle d_{x'z'}|p_{z_1'}\rangle$. We now notice that in the corundum structure, the octahedral environment of all the cation sites in a basal plane are equivalent (they are obtained from one another either by translation, or if the two cations are in the same unit cell by application of the inversion operator I, which does not change the wave functions). However, those of the next two adjacent planes are obtained by application of C_2, and subsequent translation if necessary. Under C_2 according to the definition given in Sec. IV. of I, we have, for example,

$$C_2\vec{R}_1=\vec{R}_4,$$

$$C_2(\vec{\rho}_1,\vec{\rho}_2,\vec{\rho}_3,\vec{\rho}_4,\vec{\rho}_5,\vec{\rho}_6)=(\vec{\rho}_5,\vec{\rho}_2,\vec{\rho}_4,\vec{\rho}_8,\vec{\rho}_1,\vec{\rho}_7), \qquad (2.6)$$

$$C_2(x,y,z)=(-x,y,-z),$$

where we have indicated the coordinates of the oxygen sites by ρ_i and followed the numbering of cation and anion sites as given in Fig. 1 of I.

Hence if we take the wave functions in (2.4) to be relative to the cation site $\vec{R}_1$, those relative to the site $\vec{R}_4$ will be

$$\psi^1_{\vec{R}_4}=\frac{1}{N_\pi^{1/2}}\left\{\left(\sqrt{\tfrac{2}{3}}\,d_{xy}-\sqrt{\tfrac{1}{3}}\,d_{xz}\right)-\frac{\lambda_\pi}{2\sqrt{2}}\left[\frac{2}{\sqrt{6}}(y_1-y_7-y_5+y_9)-\frac{1}{\sqrt{3}}(z_1-z_7-z_5+z_9)+\sqrt{2}\,(x_2-x_8)\right]\right\}$$

$$\begin{aligned}\psi^2_{\vec{R}_4}=\frac{1}{N_\pi^{1/2}}\Bigg\{\left(\sqrt{\tfrac{2}{3}}\,d_{y^2-x^2}+\frac{1}{\sqrt{3}}d_{yz}\right)-\frac{\lambda_\pi}{\sqrt{6}}\Bigg[&-\frac{1}{\sqrt{2}}(x_1-x_7-x_5+x_9)-\frac{2}{\sqrt{6}}(y_1-y_7+y_5-y_9)\\&-\frac{1}{2\sqrt{3}}(z_1-z_7+z_5-z_9)+\frac{1}{\sqrt{6}}(y_2-y_8)+\frac{1}{\sqrt{3}}(x_2-x_8)\Bigg]\Bigg\}\end{aligned} \qquad (2.7)$$

$$\begin{aligned}\psi^3_{\vec{R}_4}=\frac{1}{N_\pi^{1/2}}\Bigg\{d_{z^2}-\frac{\lambda_\pi}{\sqrt{12}}\Bigg[&\frac{1}{\sqrt{2}}(x_5-x_9-x_1+x_7)+\frac{1}{\sqrt{6}}(y_5-y_9+y_1-y_7)+\frac{2}{\sqrt{3}}(-z_5+z_9-z_1+z_7)\\&-\frac{2}{\sqrt{5}}(y_2-y_8)-\frac{2}{\sqrt{3}}(z_2-z_8)\Bigg]\Bigg\},\end{aligned}$$

where we have changed the sign of $\psi^1_{\vec{R}_1}$ since we want to preserve the transformation properties of the Wannier functions given in I, in which case

$$C_2\psi^1_{\vec{R}_1}=-\psi^1_{\vec{R}_4},$$

$$C_2\psi^i_{\vec{R}_1}=\psi^i_{\vec{R}_4}\quad(i=2,3), \qquad (2.8)$$

and $\psi^i_{\vec{R}_4}(i=1,2,3)$ transform under C_3 in the same way as $\psi^i_{\vec{R}_1}$.

Using this method, it is then easy to find the wave functions relative to all the other sites that are relevant for our calculations. For example the wave function centered at site 2 can be found by application of the inversion operator I such that

$$I\vec{R}_1=\vec{R}_2\,,$$
$$I(\vec{p}_1,\vec{p}_2,\vec{p}_3,\vec{p}_4,\vec{p}_5,\vec{p}_6)=(\vec{p}_{6},\vec{p}_{2'},\vec{p}_{3'},\vec{p}_{4'},\vec{p}_{5'},\vec{p}_1)\,,$$
$$I(x,y,z)=(-x,-y,-z)\,, \tag{2.9}$$

always with reference to Fig. 1 in I.

Similarly the wave function relative to the site 5 is obtained by application of C such that

$$C\vec{R}_1=\vec{R}_5\,,$$
$$C(\vec{p}_1,\vec{p}_2,\vec{p}_3,\vec{p}_4,\vec{p}_5,\vec{p}_6)=(\vec{p}_{1'},\vec{p}_{2'},\vec{p}_{3''},\vec{p}_{4''},\vec{p}_6,\vec{p}_{6''})\,,$$
$$C(x,y,z)=(x,-y,z)\,, \tag{2.10}$$

where again one has to change the sign of $\psi^1_{\vec{R}_5}$ to preserve transformation properties similar to those in (2.8).

Moreover the wave functions centered at sites $\underline{5}$ and $\underline{4}$ are simply obtained by translation from those relative to site 5 and 4. Finally the wave functions for the sites in the same basal planes of a given one but situated on adjacent vertical planes are easily obtained by the C_3 symmetry. From the knowledge of the wave functions of the type (1.1) for one site and its immediate nearest neighbors (such that the relative surrounding octahedron shares at least one oxygen with the central one) it is now possible to construct the Wannier functions (1.3) relative to a given site i. We only notice that the overlap integral S_{ij} is given by

$$S_{ij}^{mm'}=(\phi_i^m,\phi_j^{m'})-2\lambda_\pi(\phi_i^m,\chi_j^{m'})+\lambda_\pi^2(\chi_i^m,\chi_j^{m'})\,, \tag{2.11}$$

where, for example by ϕ^m ($m=1,2,3$), we indicate one of the three functions of symmetry e_g, or a_{1g} of $3d$ character in (2.4).

The effective transfer integral (1.4) is now easily calculated, since we have

$$\begin{aligned}\langle w_i^m(\vec{x})|H_0|w_j^{m'}(\vec{x})\rangle&=\langle\psi_i^m-\frac{1}{2}\sum_{nl}S_{il}^{mn}\psi_l^n|H_0|\,\psi_j^{m'}-\frac{1}{2}\sum_{n'l'}S_{jl'}^{m'n'}\psi_{l'}^{n'}\rangle\\&\cong\langle\psi_i^m|H_0|\,\psi_j^{m'}\rangle-\frac{1}{2}\sum_{n'l'}S_{jl'}^{m'n'}\langle\psi_i^m|H_0|\,\psi_{l'}^{n'}\rangle-\frac{1}{2}\sum_{nl}S_{il}^{mn}\langle\psi_l^n|H_0|\,\psi_j^{m'}\rangle\\&\cong\langle\psi_i^m|H_0|\psi_j^{m'}\rangle-\tfrac{1}{2}S_{ji}^{m'm}\langle\psi_i^m|H_0|\psi_i^m\rangle-\tfrac{1}{2}S_{ij}^{mm'}\langle\psi_j^{m'}|H_0|\psi_j^{m'}\rangle\end{aligned} \tag{2.12}$$

to first order in $S_{ij}^{mm'}$, having used the fact that $\langle\psi_i^m|H_0|\,\psi_i^{m'}\rangle=\langle\psi_i^\pi|H_0|\psi_i^\pi\rangle\delta_{mm'}$, independent of m. Hence insertion of (2.11) gives

$$\begin{aligned}\langle w_i^m(\vec{x})|H_0|\,w_j^{m'}(\vec{x})\rangle&\cong\frac{1}{N_\pi}\{\langle\phi_i^m|H_0|\phi_j^m\rangle-2\lambda_\pi[\langle\phi_i^m|H_0|\,\chi_j^{m'}\rangle-S_\pi(\phi_i^m,\chi_j^{m'})\langle\psi_i^m|H_0|\psi_i^m\rangle]\\&\qquad-\lambda_\pi^2\langle\psi_i^m|H_0|\psi_i^m\rangle\langle\chi_i^m|\chi_j^{m'}\rangle+\lambda_\pi^2\langle\chi_i^m|H_0|\chi_j^{m'}\rangle\}\\&=\frac{1}{N_\pi}\{\langle\phi_i^m|H_0|\phi_j^{m'}\rangle-2\lambda_\pi\langle\chi_i^m|\chi_j^{m'}\rangle\times[\langle\phi_i^m|H_0|\chi_i^m\rangle-S_\pi(\phi_i^m,\chi_i^m)\langle\psi_i^m|H_0|\,\psi_i^m\rangle]-\lambda_\pi^2\langle\chi_i^m|\,\chi_j^{m'}\rangle\\&\qquad\times[\langle\psi_i^m|H_0|\,\psi_i^m\rangle-\langle\chi_i^m|H_0|\chi_i^m\rangle]\}\,,\end{aligned} \tag{2.13}$$

where we have used the property that

$$\begin{aligned}\langle\chi_i^m|H_0|\,\chi_j^{m'}\rangle&=\langle\chi_i^m|H_0|\chi_i^m\rangle\langle\chi_i^m|\chi_j^{m'}\rangle\,,\\\langle\phi_i^m|H_0|\chi_j^{m'}\rangle&=\langle\phi_i^m|H_0|\chi_i^m\rangle\langle\chi_i^m|\chi_j^{m'}\rangle\,,\\S_\pi(\phi_i^m,\chi_j^{m'})&=S_\pi(\phi_i^m,\chi_i^m)\langle\chi_i^m|\,\chi_j^{m'}\rangle\,,\end{aligned} \tag{2.14}$$

provided overlap between oxygens is neglected. This property follows from the fact that for the $2p_\pi$ oxygen orbitals relative to those sites which are in common to the two octahedra centered at i and j, the set of function $\chi_{i\pi}^m$ of symmetry $t_{1u}, t_{2g}, t_{1g}, t_{2u}$ is complete and the fact that, for example, $(\phi_i^m|H_0|\chi_i^{m'})=0$ unless the symmetry type of the two functions is the same.

If we now, in Eq. (2.13), remember the result of ligand field theory,[11] that

$$-\lambda_\pi=\frac{\langle\phi_i|H_0|\chi_i\rangle-S_\pi(\phi_i,\chi_i)\langle\psi_i|H_0|\psi_i\rangle}{\langle\psi_i|H_0|\psi_i\rangle-\langle\chi_i|H_0|\chi_i\rangle} \tag{2.15}$$

and put the denominator in this last expression equal to $E_{3d}-E_{2p}=\Delta E$, the energy difference between the $3d$ antibonding states and the $2p_\pi t_{2g}$ bonding states, we end up with the formula (1.4). Notice that in this derivation we have neglect the first term in (2.11) which is usually much smaller than the other ones.

It can be shown[12] that this derivation of the effective transfer integral is exact up to second order in λ_π (remember that already $S_{ij}^{mm'}$ is second order in λ_π) and is actually the result of second-order perturbation theory when one tries to eliminate from the problem the ligands and uses an effective Hamiltonian for the $3d$ antibonding bond. Before going on to calculate the effective transfer integrals of a site to its immediate neighbors we want just notice that from the way we have constructed them, our Wannier functions transform as the set xy, xz, yz, so that the property (2.9) of I follows.

Figure 9 in I represents a characteristic cluster of *V* atoms with corundum structure showing the site 1 connected with all its neighbors whose oxygen cluster shares at least one oxygen with the central ones around 1. The relative transfer integrals are given in Table I. These latter are all obtained in terms of twelve quantities which, according to Eq. (1.4) have the following expression:

$$
\begin{aligned}
&\mu = (1/N_\pi)[\tfrac{1}{3}\lambda_\pi^2 \Delta E + \langle \phi_{\vec{R}_1}^{1(2)} | H_0 | \phi_{\vec{R}_4}^{1(2)} \rangle], \quad \nu = -(1/N_\pi \tfrac{1}{24}\lambda_\pi^2 \Delta E,\\
&-\alpha = (1/N_\pi)\,[-\tfrac{1}{4}\lambda_\pi^2 \Delta E + \langle \phi_{\vec{R}_1}^{1} | H_0 | \phi_{\vec{R}_2}^{1} \rangle], \quad \pi = (1/N_\pi)\tfrac{1}{72}\lambda_\pi^2 \Delta E,\\
&\beta = (1/N_\pi)[\tfrac{1}{12}\lambda_\pi^2 \Delta E + \langle \phi_{\vec{R}_1}^{2} | H_0 | \phi_{\vec{R}_2}^{2} \rangle], \quad \delta = (1/N_\pi)(5/24\sqrt{3})\lambda_\pi^2 \Delta E,\\
&\rho = (1/N_\pi)[-\tfrac{1}{6}\lambda_\pi^2 \Delta E + \langle \phi_{\vec{R}_1}^{3} | H_0 | \phi_{\vec{R}_4}^{3} \rangle], \quad \epsilon = -(1/N_\pi)\tfrac{5}{36}\lambda_\pi^2 \Delta E,\\
&\sigma = (1/N_\pi)[\tfrac{1}{6}\lambda_\pi^2 \Delta E + \langle \phi_{\vec{R}_1}^{3} | H_0 | \phi_{\vec{R}_2}^{3} \rangle], \quad \lambda = (1/N_\pi)(1/12\sqrt{6})\lambda_\pi^2 \Delta E,\\
&-\tau = (1/N_\pi)[-(1/6\sqrt{2})\lambda_\pi^2 \Delta E + \langle \phi_{\vec{R}_1}^{3} | H_0 | \phi_{\vec{R}_2}^{2} \rangle], \quad \omega = -(1/N_\pi)(7/36\sqrt{2})\lambda_\pi^2 \Delta E.
\end{aligned}
\tag{2.16}
$$

Here the numerical coefficients are the quantities $(\chi_i^m | \chi_j^{m'})$ which can be easily calculated on the basis of the ligand wave functions in (2.4), (2.7), or those derived therefrom. For the second set of (2.16) we have neglected the direct transfer integral between 3*d* wave functions since the relative sites are at a distance of about 4 Å in the corundum structure. For the first set we easily calculate, using the notations and Table I of the paper by Slater and Koster,[13]

TABLE I. Transfer integrals $t_{mm'}(m, m' = 1, 2, 3)$ along direction δ and between orbitals m and m' where $(m, m' = 1, 2)$ indicates the two Wannier states of e_g symmetry and $(m, m' = 3)$ of a_{1g} symmetry.

Direction Transfer integral	δ_4	δ_2	$\delta_{3'}$	δ_3	δ_5	$\delta_{6'}$	δ_6	$\delta_{\underline{4}}$
t_{11}	μ	$-\alpha$	$-\frac{1}{4}\alpha+\frac{3}{4}\beta$	$-\frac{1}{4}\alpha+\frac{3}{4}\beta$	ν	$\frac{1}{4}\nu+\frac{3}{4}\pi$	$\frac{1}{4}\nu+\frac{3}{4}\pi$	ν
t_{22}	μ	β	$-\frac{3}{4}\alpha+\frac{1}{4}\beta$	$-\frac{3}{4}\alpha+\frac{1}{4}\beta$	π	$\frac{3}{4}\nu+\frac{1}{4}\pi$	$\frac{3}{4}\nu+\frac{1}{4}\pi$	π
t_{33}	ρ	σ	σ	σ	$\underline{\epsilon}$	$\underline{\epsilon}$	ϵ	$\underline{\epsilon}$
t_{12}	0	0	$\frac{1}{4}\sqrt{3}(\alpha+\beta)$	$-\frac{1}{4}\sqrt{3}(\alpha+\beta)$	δ	$\frac{1}{4}\sqrt{3}(-\nu+\pi)+\delta$	$-\frac{1}{4}\sqrt{3}(-\nu+\pi)+\delta$	$-\delta$
t_{13}	0	0	$\frac{1}{2}\sqrt{3}\,\tau$	$-\frac{1}{2}\sqrt{3}\,\tau$	λ	$-\frac{1}{2}\sqrt{3}\,\omega-\frac{1}{2}\lambda$	$\frac{1}{2}\sqrt{3}\,\omega-\frac{1}{2}\lambda$	$-\lambda$
t_{23}	0	$-\tau$	$\frac{1}{2}\tau$	$\frac{1}{2}\tau$	ω	$-\frac{1}{2}\omega+\frac{1}{2}\sqrt{3}\lambda$	$-\frac{1}{2}\omega-\frac{1}{2}\sqrt{3}\lambda$	ω
t_{21}	0	0	$\frac{1}{4}\sqrt{3}(\alpha+\beta)$	$-\frac{1}{4}\sqrt{3}(\alpha+\beta)$	$-\delta$	$\frac{1}{4}\sqrt{3}(-\nu+\pi)-\delta$	$-\frac{1}{4}\sqrt{3}(-\nu+\pi)-\delta$	δ
t_{31}	0	0	$\frac{1}{2}\sqrt{3}\,\tau$	$-\frac{1}{2}\sqrt{3}\,\tau$	$-\lambda$	$\frac{1}{2}\sqrt{3}\,\omega+\frac{1}{2}\lambda$	$-\frac{1}{2}\sqrt{3}\,\omega+\frac{1}{2}\lambda$	λ
t_{32}	0	$-\tau$	$\frac{1}{2}\tau$	$\frac{1}{2}\tau$	ω	$-\frac{1}{2}\omega-\frac{1}{2}\sqrt{3}\lambda$	$-\frac{1}{2}\omega+\frac{1}{2}\sqrt{3}\lambda$	ω

Direction Transfer integral	$\delta_{\underline{8}'}$	$\delta_{\underline{8}}$	$\delta_{\underline{5}}$	$\delta_{\underline{6}'}$	$\delta_{\underline{6}}$
t_{11}	$\frac{1}{4}\nu+\frac{3}{4}\pi$	$\frac{1}{4}\nu+\frac{3}{4}\pi$	ν	$\frac{1}{4}\nu+\frac{3}{4}\pi$	$\frac{1}{4}\nu+\frac{3}{4}\pi$
t_{22}	$\frac{3}{4}\nu+\frac{1}{4}\pi$	$\frac{3}{4}\nu+\frac{1}{4}\pi$	π	$\frac{3}{4}\nu+\frac{1}{4}\pi$	$\frac{3}{4}\nu+\frac{1}{4}\pi$
t_{33}	ϵ	ϵ	ϵ	ϵ	ϵ
t_{12}	$\frac{1}{4}\sqrt{3}(-\nu+\pi)-\delta$	$\frac{1}{4}\sqrt{3}(-\nu+\pi)-\delta$	δ	$-\frac{1}{4}\sqrt{3}(-\nu+\pi)+\delta$	$\frac{1}{4}\sqrt{3}(-\nu+\pi)+\delta$
t_{13}	$-\frac{1}{2}\sqrt{3}\omega+\frac{1}{2}\lambda$	$-\frac{1}{2}\sqrt{3}\,\omega+\frac{1}{2}\lambda$	λ	$\frac{1}{2}\sqrt{3}\,\omega-\frac{1}{2}\lambda$	$-\frac{1}{2}\sqrt{3}\,\omega-\frac{1}{2}\lambda$
t_{23}	$-\frac{1}{2}\omega+\frac{1}{2}\sqrt{3}\lambda$	$-\frac{1}{2}\omega-\frac{1}{2}\sqrt{3}\lambda$	ω	$-\frac{1}{2}\omega-\frac{1}{2}\sqrt{3}\lambda$	$-\frac{1}{2}\omega+\frac{1}{2}\sqrt{3}\lambda$
t_{21}	$-\frac{1}{4}\sqrt{3}(-\nu+\pi)+\delta$	$\frac{1}{4}\sqrt{3}(-\nu+\pi)+\delta$	$-\delta$	$-\frac{1}{4}\sqrt{3}(-\nu+\pi)-\delta$	$\frac{1}{4}\sqrt{3}(-\nu+\pi)-\delta$
t_{31}	$-\frac{1}{2}\sqrt{3}\,\omega-\frac{1}{2}\lambda$	$\frac{1}{2}\sqrt{3}\,\omega-\frac{1}{2}\lambda$	$-\lambda$	$-\frac{1}{2}\sqrt{3}\,\omega+\frac{1}{2}\lambda$	$\frac{1}{2}\sqrt{3}\,\omega+\frac{1}{2}\lambda$
t_{32}	$-\frac{1}{2}\omega-\frac{1}{2}\sqrt{3}\lambda$	$-\frac{1}{2}\omega+\frac{1}{2}\sqrt{3}\lambda$	ω	$-\frac{1}{2}\omega+\frac{1}{2}\sqrt{3}\lambda$	$-\frac{1}{2}\omega-\frac{1}{2}\sqrt{3}\lambda$

$$\langle\phi^{1(2)}_{\vec{R}_1}|H_0|\phi^{1(2)}_{\vec{R}_4}\rangle = \tfrac{2}{3}(dd\delta)_{14} - \tfrac{1}{3}(dd\pi)_{14} \simeq -0.16 \text{ eV},$$
$$\langle\phi^{1}_{\vec{R}_1}|H_0|\phi^{1}_{\vec{R}_2}\rangle = \tfrac{2}{3}(dd\pi)_{12} + \tfrac{1}{3}(dd\delta)_{12} \simeq 0.14 \text{ eV},$$
$$\langle\phi^{2}_{\vec{R}_1}|H_0|\phi^{2}_{\vec{R}_2}\rangle = \tfrac{1}{2}(dd\sigma)_{12} + \tfrac{1}{3}(dd\pi)_{12} + \tfrac{1}{6}(dd\delta)_{12} \simeq -0.15 \text{ eV}, \qquad (2.17)$$
$$\langle\phi^{3}_{\vec{R}_1}|H_0|\phi^{3}_{\vec{R}_4}\rangle = (dd\sigma)_{14} \simeq -0.66 \text{ eV},$$
$$\langle\phi^{3}_{\vec{R}_1}|H_0|\phi^{3}_{\vec{R}_2}\rangle = \tfrac{1}{4}(dd\sigma)_{12} + \tfrac{3}{4}(dd\delta)_{12} \simeq -0.14 \text{ eV},$$
$$\langle\phi^{3}_{\vec{R}_1}|H_0|\phi^{2}_{\vec{R}_2}\rangle = \tfrac{1}{4}\sqrt{2}\,(dd\sigma)_{12} - \tfrac{1}{4}\sqrt{2}\,(dd\delta)_{12} \simeq -0.14 \text{ eV}.$$

The orientative values in (2.17) are estimated on the basis of Table II of Ref. 5 where the same Slater-Koster notation is used and the sites labeled $\vec{R}_1, \vec{R}_4, \vec{R}_2, \vec{R}_5$ are called c_0, b_0, d_0, a_0, respectively. Notice that the distance $|\vec{R}_1 - \vec{R}_4|$ is different from $|\vec{R}_1 - \vec{R}_2|$ so that for example we have to distinguish between $(dd\pi)_{14}$ and $(dd\pi)_{12}$.

All the other transfer integrals centered at any other cation site in the unit cell are obtained from those of Table I by application of the symmetry operations I, C_2, or C, as exemplified in Sec. IV of I.

Before leaving this section we want to point out the importance of covalency effects as it emerges from (2.16), (2.17). With values for λ_π^2 ranging from 0.25 to 0.40 and for ΔE between 4 and 5 eV we see that interference effects between direct $3d$-$3d$ transfer integral, and covalency contribution are crucial in determining the effective hopping rate of the electrons from site to site. The interplay between the effective possibility of maximum lowering of the kinetic energy for the electrons and the minimum paying of repulsive energy when they happen to be on the same site determine the electronic structure and the distances between the anions and the cations among themselves and between anions and cations. Also notice that covalency alone can be a big non-negligible source of hopping between sites so that it is essential to take it into account for a correct treatment of the problem.

We shall return later to these points when discussion the correlations between electrons in the corundum structure for the series Ti_2O_3, V_2O_3, and Cr_2O_3.

III. UNRESTRICTED HARTREE-FOCK CALCULATION

As already anticipated in the introduction, we shall make use of the Green's-function technique to perform an unrestricted Hartree-Fock calculation for V_2O_3. Our aim will be the calculation of the ground-state energy in order to assess the goodness of the type of correlations introduced in the trial wave function which in the language of the Green's-function technique are all contained in the set of the self-consistent occupation numbers $\langle n_{i\alpha m\sigma}\rangle$ relative to the r sites α in the unit cell, the symmetry type index $m(=1, 2, 3)$, and the spin σ.

It is then natural to start with a general expression of the average of the operator $H - \mu N$ in a grand canonical ensemble in terms of correlation functions,[14] namely,

$$\langle H - \mu N\rangle = \frac{1}{4}\sum_{\sigma}\int d^3x \Big| \left[i\frac{\partial}{\partial t} - i\frac{\partial}{\partial t'} + H_0(\vec{x}') + H_0(\vec{x}) - 4\mu \right] \langle\psi^\dagger_\sigma \vec{x}', t')\psi_\sigma(\vec{x}, t)\rangle \Big|_{\substack{\vec{x}=\vec{x}' \\ t=t'}}, \qquad (3.1)$$

where $H_0(\vec{x}) = (-\hbar^2/2m)\nabla^2_{\vec{x}} + V(\vec{x})$ is the one-body part of the total Hamiltonian, and then to specialize to our case in order to fix the notations and have expressions ready for direct calculations. Eq. (3.1) is easily obtained by eliminating the two-particle correlation functions coming from the interaction part of the Hamiltonian through the equation of motion of the field operator itself.

Let us expand the field operator

$$\psi_\sigma(\vec{x}, t) = \sum_{i\alpha m} w^m_{i\alpha}(\vec{x}) c_{i\alpha m\sigma}(t) \qquad (3.2)$$

in terms of operators which annihilate electrons in real Wannier states $w^m_{i\alpha}(\vec{x})$ relative to the lattice site $\vec{R}_i + \vec{x}_\alpha$ (R_i denoting the primitive unit cell and $\vec{x}_\alpha$ the position of the site within this cell and to the mth type of symmetry (or mth atomic level). Introducing the Fourier transform of the averages

$$\langle c^\dagger_{a'}(t')c_a(t)\rangle = \int_{-\infty}^{+\infty}\frac{d\omega}{2\pi} e^{-i\omega(t-t')} G^<_{c_a c^\dagger_{a'}}(\omega), \quad a = i\alpha m\sigma, \qquad (3.3)$$

in the usual notations and the quantities

$$T_{a',a} = \int w_{a'}(\vec{x}) H_0(\vec{x}) w_a(\vec{x}) d^3x, \quad a = i\alpha m, \qquad (3.4)$$

the expression (3.1) becomes

$$\langle H - \mu N\rangle = \frac{1}{4}\sum_{i\alpha}\sum_{i'\alpha'}\sum_{mm'}\sum_{\sigma}\int\frac{d\omega}{2\pi}\left[2(\omega - 2\mu)\delta_{i\alpha m, i'\alpha' m'} + 2T^{m'm}_{i'\alpha', i\alpha}\right] G^<(i\alpha m\sigma, i'\alpha' m'\sigma; \omega), \qquad (3.5)$$

where we have put for brevity $G^<_{c_a c^\dagger_{a'}}(\omega) \equiv G^<(a, a'; \omega)$. Fourier transforming in space (N_c being the total number of unit cells and $\vec{k}$ varying in the first Brillouin zone)

$$c_{i\alpha m\sigma}=\frac{1}{\sqrt{N_c}}\sum_{k'} e^{+i\vec{k}\cdot(\vec{R}_i+\vec{x}_\alpha)}c_{\vec{k}\alpha m\sigma}, \tag{3.6}$$

so that

$$G^<(i\alpha m\sigma, i'\alpha'm'\sigma';\omega)=\frac{1}{N_c}\sum_{\vec{k}} G^<(\alpha m\sigma,\alpha'm'\sigma';\vec{k};\omega)e^{+i\vec{k}\cdot(\vec{R}_i-\vec{R}_{i'}+\vec{x}_\alpha-\vec{x}_{\alpha'})},$$

we obtain

$$\langle H-\mu N\rangle=\frac{1}{2}\sum_{\vec{k}}\sum_{\alpha m\sigma}\sum_{\alpha'm'}\int_{-\infty}^{\infty}\frac{d\omega}{2\pi}[(\omega-2\mu)\delta_{\alpha m,\alpha'm'}+T^{m'm}_{\alpha',\alpha}(\vec{k})]G^<(\alpha m\sigma,\alpha'm'\sigma;\vec{k};\omega), \tag{3.7}$$

where we have introduced the quantity

$$T^{m'm}_{\alpha',\alpha}(\vec{k})=\sum_{i'}T^{m'm}_{i'\alpha',i\alpha}e^{i\vec{k}\cdot(\vec{R}_i+\vec{x}_\alpha-\vec{R}_{i'}-\vec{x}_{\alpha'})} \tag{3.8}$$

which is independent of i because of the translational invariance. It is useful to write Eq. (3.7) in matrix notation upon introduction of the matrices

$$\begin{aligned}&\underline{I}=(\delta_{\alpha m\sigma,\alpha'm'\sigma'}),\\&\underline{T}(\vec{k})=(T^{m'm}_{\alpha',\alpha}(\vec{k})\delta_{\sigma\sigma'}),\\&\underline{G}^<(\vec{k};\omega)\equiv(G^<(\alpha m\sigma,\alpha'm'\sigma';\vec{k};\omega))\end{aligned} \tag{3.9}$$

so that

$$\begin{aligned}\langle H-\mu N\rangle&=\frac{1}{2}\sum_{\vec{k}}\mathrm{Tr}\int_{-\infty}^{+\infty}\frac{d\omega}{2\pi}[(\omega-2\mu)\underline{I}+\underline{T}(\vec{k})]\underline{G}^<(\vec{k};\omega)\\&=\frac{1}{2}\sum_{\vec{k}}\mathrm{Tr}\int_{-\infty}^{+\infty}\frac{d\omega}{2\pi}[(\omega-2\mu)\underline{I}+\underline{T}(\vec{k})]f(\omega)\underline{A}(\vec{k};\omega),\end{aligned} \tag{3.10}$$

with $f(\omega)=[\exp\beta(\omega-\mu)+1]^{-1}$, $\underline{A}(\vec{k};\omega)$ being the matrix of the spectral functions of the Zubarev Green functions

$$\langle\langle c_{\vec{k}\alpha m\sigma};c^\dagger_{\vec{k}\alpha'm'\sigma'}\rangle\rangle .$$

The symbol Tr indicates that the trace of the matrix product on the right should be taken.

Until now Eq. (3.10) is generally valid. We turn next to the approximate evaluation of the above Green's function. We start from the Hamiltonian (2.3) of I which we repeat here for convenience.

$$\begin{aligned}H=\sum_{j\sigma'}\sum_{mm'\sigma}t^{mm'}_{jj'}c^\dagger_{jm\sigma}c_{j'm'\sigma}+\frac{1}{2}\sum_{j}\sum_{mm'}\sum_{\sigma\sigma'}[&(1-\delta_{mm'}\delta_{\sigma\sigma'})U_{mm'}n_{jm\sigma}n_{jm'\sigma'}-\delta_{\sigma\sigma'}(1-\delta_{mm'})J_{mm'}n_{jm\sigma}n_{jm'\sigma}\\&-(1-\delta_{mm'})(1-\delta_{\sigma\sigma'})J_{mm'}c^\dagger_{jm\sigma}c_{jm\sigma'}c^\dagger_{jm'\sigma'}c_{jm'\sigma}\\&+(1-\delta_{mm'})(1-\delta_{\sigma\sigma'})J_{mm'}c^\dagger_{jm'\sigma'}c^\dagger_{jm'\sigma}c_{jm\sigma'}],\end{aligned} \tag{3.11}$$

where j stands for $i\alpha$ defined above and the sum over m, and m' goes over the three Wannier states per site defined in Sec. II. We remind ourselves of the following definitions:

$$U_{mm'}=U\delta_{mm'}+U'(1-\delta_{mm'}),\quad J_{mm'}=J(1-\delta_{mm'}) \tag{3.12}$$

and

$$U=U'+2J. \tag{3.13}$$

Notice that the generalized Hubbard Hamiltonian, beside neglecting the long-range part of the Coulomb interaction, neglects also exchange terms between neighbor sites. These favor ferromagnetic coupling between electrons and might to some extent compete with kinetic exchange mechanism, although we believe Anderson's[2] argument that interference effects tend to depress their value. For this reason we neglected them here.

The equation of motion for $\langle\langle c_{jm\sigma};c^\dagger_{j'm'\sigma'}\rangle\rangle$ is

$$\begin{aligned}\omega\langle\langle c_{jm\sigma};c^+_{j'm'\sigma'}\rangle\rangle=&\langle\{c_{jm\sigma},c^+_{j'm'\sigma'}\}\rangle\\&+\langle\langle[c_{jm\sigma},H];c^+_{j'm'\sigma'}\rangle\rangle,\end{aligned} \tag{3.14}$$

that is to say

$$\begin{aligned}\omega\langle\langle c_{jm\sigma};c^{\dagger}_{j'm'\sigma'}\rangle\rangle &= \delta_{jm\sigma,j'm'\sigma'}+\sum_{ln}t^{mn}_{jl}\langle\langle c^{\dagger}_{ln\sigma};\rangle\rangle+\sum_{ns}(1-\delta_{mn}\delta_{\sigma s})U_{mn}\langle\langle c^{\dagger}_{jm\sigma}n_{jns};\rangle\rangle\\ &\quad-\sum_{ns}(1-\delta_{mn})(1-\delta_{\sigma s})J_{mn}\langle\langle c^{\dagger}_{jms}c^{\dagger}_{jn\,-s}c_{jns};\rangle\rangle-\sum_{n}(1-\delta_{mn})J_{mn}\langle\langle c^{\dagger}_{jm\sigma}n_{jn\sigma};\rangle\rangle\\ &\quad+\sum_{ns}(1-\delta_{mn})(1-\delta_{\sigma s})J_{mn}\langle\langle c^{\dagger}_{jn\sigma}c^{\dagger}_{jns}c_{jms};\rangle\rangle\,,\end{aligned}\tag{3.15}$$

where we have omitted for brevity the second operator in the Green's functions.

The unrestricted Hartree-Fock approximation demands that we decouple the higher-order Green's functions in (3.15) by taking into consideration all the possible nonzero averages of the form $\langle c^{+}_{jm\sigma}c_{jn\sigma}\rangle$. We suppose that all the spins are aligned along the quantization axis so that

$$\langle c^{+}_{jm\sigma}c_{jns}\rangle=\langle c^{+}_{jm\sigma}c_{jn\sigma}\rangle\delta_{\sigma s}\ .$$

For example,

$$\langle\langle c^{\dagger}_{jm\sigma}n_{jns};\rangle\rangle\cong-\langle c^{\dagger}_{jm\sigma}c_{jns}\rangle\langle\langle c_{jns};\rangle\rangle+\langle n_{jns}\rangle\langle\langle c^{\dagger}_{jm\sigma};\rangle\rangle\,.\tag{3.16}$$

Performing all the possible decouplings in (3.15) and Fourier transforming according to (3.6) (resetting $j=i,\ \alpha$) we finally obtain

$$\begin{aligned}\omega\langle\langle c_{\vec{k}\alpha m\sigma};c^{\dagger}_{\vec{k}\beta m'\sigma'}\rangle\rangle&=\delta_{\alpha\beta}\delta_{mm'}\delta_{\sigma\sigma'}\\&\quad+\sum_{n\gamma}[T^{mn}_{\alpha,\gamma}(\vec{k})+\Lambda^{mn}_{\alpha,\gamma}]\\&\qquad\times\langle\langle c_{\vec{k}\gamma n\sigma};c^{\dagger}_{\vec{k}\beta m'\sigma'}\rangle\rangle\,,\end{aligned}\tag{3.17}$$

where we have defined the interaction matrix

$$\begin{aligned}\Lambda^{mn}_{\alpha,\gamma}=\delta_{\alpha\gamma}\{&[U\langle n_{\alpha m\,-\sigma}\rangle+U'\sum_{n's}(1-\delta_{mn'})\langle n_{\alpha n's}\rangle\\&-J\sum_{n'}(1-\delta_{mn'})\langle n_{\alpha n'\sigma}\rangle]\delta_{mn}\\&-[(U'-J)\langle c^{\dagger}_{\alpha m\sigma}c_{\alpha n\sigma}\rangle\\&\quad-J(\langle c^{\dagger}_{\alpha n\,-\sigma}c_{\alpha m\,-\sigma}\rangle+\langle c^{\dagger}_{\alpha m\,-\sigma}c_{\alpha n\,-\sigma}\rangle)]\}\,.\end{aligned}\tag{3.18}$$

Notice that we have dropped the index i in the averages like $\langle n_{i\alpha m\sigma}\rangle$ since by translation invariance these latter do not depend on i (remember that i denotes the unit cell). Defining the matrices

$$\begin{aligned}&\underline{G}(\vec{k};\omega)=(\langle\langle c_{\vec{k}\alpha m\sigma};c^{\dagger}_{\vec{k}\beta m'\sigma'}\rangle\rangle)\,,\\&\underline{C}(\vec{k}|\langle n_{\alpha}\rangle)\equiv[T^{mn}_{\alpha,\gamma}(\vec{k})+\Lambda^{mn}_{\alpha,\gamma}]\delta_{\sigma,\sigma'}\,,\end{aligned}\tag{3.19}$$

where we have indicated that the matrix C depends on the set $\langle n_a\rangle(a=\gamma ns)$, we can rewrite (3.17) as

$$(\omega\underline{I}-\underline{C})\underline{G}=\underline{I}\,.\tag{3.20}$$

To find the self-consistent equations for the occupation numbers $\langle n_a\rangle$, the unitary matrix $\underline{V}$ of the eigenvectors of the matrix $\underline{C}$ is first found. So,

$$\underline{V}\equiv(V_{\gamma ns,\lambda})\,,\tag{3.21}$$

where

$$\sum_{\gamma ns}C_{\alpha m\sigma,\gamma ns}V_{\gamma ns,\lambda}=\omega_{\lambda}V_{\alpha m\sigma,\lambda}\,,\tag{3.22}$$

and

$$\sum_{\alpha m\sigma}V^{*}_{\alpha m\sigma,\lambda}V_{\alpha m\sigma,\lambda'}=\delta_{\lambda\lambda'}\ \text{i.e.}\ \underline{V}^{\dagger}\underline{V}=\underline{I}\,.\tag{3.23}$$

(We have assumed that in case of degeneracy a suitable orthonormal basis in the subspace of the degenerate eigenvalue has been chosen.) Hence,

$$\underline{V}^{\dagger}\underline{C}\,\underline{V}=\Omega\,,\tag{3.24}$$

where

$$\Omega\equiv(\omega_{\lambda}\delta_{\lambda\lambda'})\,,\tag{3.25}$$

so that by multiplication of (3.20) by $\underline{V}^{\dagger}$ from the left and by $\underline{V}$ from the right, we derive

$$(\omega\underline{I}-\Omega)\underline{G}'=\underline{I}\,,\tag{3.26}$$

where

$$\underline{G}'=\underline{V}^{\dagger}\underline{G}\,\underline{V}\,.\tag{3.27}$$

The solution for $\underline{G}'$ is easily obtained as

$$\underline{G}'\equiv[1/(\omega-\omega_{\lambda})]\ \ \delta'_{\lambda\lambda}\tag{3.28}$$

so that

$$\underline{G}=\underline{V}\,\underline{G}'\underline{V}^{\dagger}\equiv\left(\sum_{\lambda}\frac{V_{\alpha m\sigma,\lambda}V^{*}_{\gamma ns,\lambda}}{\omega-\omega_{\lambda}}\right).\tag{3.29}$$

Hence

$$\begin{aligned}\underline{A}(\vec{k};\omega)&=i[\underline{G}(\vec{k};\omega+i\epsilon)-\underline{G}(\vec{k};\omega-i\epsilon)]\\&\equiv\left(2\pi\sum_{\lambda}V_{\alpha m\sigma,\lambda}(\vec{k})V^{*}_{\gamma ns,\lambda}(\vec{k})\delta(\omega-\omega_{\lambda'}(\vec{k}))\right),\end{aligned}\tag{3.30}$$

so that for the self-consistent equations we have

$$\langle c^{\dagger}_{\alpha m\sigma}c_{\alpha n\sigma}\rangle=\frac{1}{N_c}\sum_{\vec{k}}\sum_{\lambda}V^{*}_{\alpha m\sigma,\lambda}(\vec{k})V_{\alpha n\sigma,\lambda}(\vec{k})\times\left(\exp\{\beta[\omega_\lambda(\vec{k})-\mu]\}+1\right)^{-1};\tag{3.31}$$

and the chemical potential μ is determined from the condition that

$$n_c=\sum_{\alpha m\sigma}\langle c^{\dagger}_{\alpha m\sigma}c_{\alpha m\sigma}\rangle=\frac{1}{N_c}\sum_{\vec{k}}\sum_{\lambda}\left(\exp\{\beta[\omega_\lambda(\vec{k})-\mu]\}+1\right)^{-1},\tag{3.32}$$

where n_c is the total number of electrons per unit cell, having used Eq. (3.23).

In simple cases, where the $V_{\alpha m\sigma,\lambda},(\vec{k})$ can be obtained analytically, relation (3.31) is easily recognized to be the usual self-consistent equation. For example, in the case of two sites α and β per unit cell and one atomic state ($m=1$) (with only nearest-neighbor transfer integrals different from zero), Eq. (3.31) reads, at $T=0$,

$$\begin{aligned}\langle n_{\alpha\sigma}\rangle&=\tfrac{1}{2}\left(1-\frac{1}{N_c}\sum_{\vec{k}}\frac{\langle n^{-}_{-\sigma}\rangle}{(\langle n^{-}_{-\sigma}\rangle^{2}+\rho^{2}\gamma^{2}_{\vec{k}})^{1/2}}\right),\\ \langle n_{\beta\sigma}\rangle&=\tfrac{1}{2}\left(1+\frac{1}{N_c}\sum_{\vec{k}}\frac{\langle n^{-}_{-\sigma}\rangle}{(\langle n^{-}_{-\sigma}\rangle^{2}+\rho^{2}\gamma^{2}_{\vec{k}})^{1/2}}\right),\end{aligned}\tag{3.33}$$

where

$$\langle n^{-}_{\sigma}\rangle=\langle n_{\alpha\sigma}\rangle-\langle n_{\beta\sigma}\rangle\,,$$

$$\rho=W/U=2zt/U\,,$$

and

$$\gamma_{\vec{k}}=\frac{1}{z}\sum_{\langle\alpha\beta\rangle}e^{i\vec{k}\cdot\vec{\delta}_{\alpha\beta}}\,.$$

Subtracting, we get

$$\langle n^{-}_{\sigma}\rangle=-\frac{1}{N_c}\sum_{\vec{k}}\frac{\langle n^{-}_{-\sigma}\rangle}{(\langle n_{-\sigma}\rangle^{2}+\rho^{2}\gamma^{2}_{\vec{k}})^{1/2}},\tag{3.34}$$

which is seen to be the self-consistent equation in Ref. 9 for $T=0$. In the more general case, Eq. (3.31) is already suitable for computer calculations. A suitable set of input occupations numbers as suggested by our preceding atomic calculations is used to construct the $\underline{C}$ matrix in (3.19). Next, an orthonormal set of eigenvectors is found at each one of a suitable number of $\vec{k}$ points in the irreducible part of the Brillouin zone (BZ) (250 is usually found to be sufficient) and the sum (3.31) is performed together with the sum (3.32) which determines the Fermi level. Hence a new set of occupation numbers is obtained which is used as a new input set to repeat the procedure. It can be shown that this procedure converges to a self-consistent set of solutions. In general, as suggested by the atomic calculation, there is a great variety of such self-consistent solutions. To discriminate among them it is necessary to calculate the corresponding ground-state energy in order to assess the most stable configuration.

From Eq. (3.10) we get, with $\underline{\Lambda}=(\Lambda^{mn}_{\alpha,\gamma}\delta_{\sigma,\sigma'})$,

$$\begin{aligned}\langle H-\mu N\rangle&=\tfrac{1}{2}\sum_{\vec{k}}\mathrm{Tr}\int_{-\infty}^{+\infty}\frac{d\omega}{2\pi}[(\omega-2\mu)\underline{I}+\underline{T}(\vec{k})]f(\omega)\underline{A}(\vec{k};\omega)\\&=\tfrac{1}{2}\sum_{\vec{k}}\mathrm{Tr}\int_{-\infty}^{+\infty}\frac{d\omega}{2\pi}[(\omega-2\mu)\underline{I}+\underline{T}(\vec{k})+\underline{\Lambda}]f(\omega)\underline{A}(\vec{k};\omega)\\&\quad-\tfrac{1}{2}\sum_{\vec{k}}\mathrm{Tr}\int_{-\infty}^{+\infty}\frac{d\omega}{2\pi}\underline{\Lambda}f(\omega)\underline{A}(\vec{k};\omega)\,.\end{aligned}\tag{3.35}$$

Using the unitary matrix $\underline{V}$ to evaluate the first trace and remembering (3.31), we obtain

$$\begin{aligned}\frac{1}{N_c}\langle H-\mu N\rangle=&\frac{1}{N_c}\sum_{\vec{k}}\sum_{\lambda}[\omega_\lambda(\vec{k})-\mu)](\exp\{\beta[\omega_\lambda(\vec{k})-\mu]\}+1)^{-1}\\&-\frac{1}{2}\sum_{\alpha m\sigma}\langle n_{\alpha m\sigma}\rangle[U\langle n_{\alpha m-\sigma}\rangle+U'\sum_{n\sigma'}(1-\delta_{mn})\langle n_{\alpha n\sigma'}\rangle-J\sum_{n}(1-\delta_{mn})\langle n_{\alpha n\sigma}\rangle]\\&+\frac{1}{2}\sum_{\alpha\sigma}\sum_{mn}(1-\delta_{mn})\langle c^{\dagger}_{\alpha n\sigma}c_{\alpha m\sigma}\rangle[(U-J)\langle c^{\dagger}_{\alpha m\sigma}c_{\alpha n\sigma}\rangle-J(\langle c^{\dagger}_{\alpha n-\sigma}c_{\alpha m-\sigma}\rangle+\langle c^{\dagger}_{\alpha m-\sigma}c_{\alpha n-\sigma}\rangle)]\end{aligned}\tag{3.36}$$

for the total energy per unit cell. We recognize in this equation the usual expression for the ground-state energy in the Hartree-Fock approximation.

In practice, since the matrix $\underline{C}$ in (3.19) is diagonal in the spin indices, the diagonalization (3.22) is done for each spin state so that ω_λ can be indexed as $\omega_{\lambda'\sigma}$ (where if λ ranges from 1 to n, λ' ranges from 1 to $\frac{1}{2}n$). This has the advantage that in the antiferromagnetic spin structures one saves computation time since $\omega_{\lambda'\sigma}$ is independent of σ. In such a case, the set for down-spin occupation numbers can be obtained from that of up-spin by a suitable symmetry operation inside the unit cell. Finally we want to comment on the connection of the usual variational Hartree-Fock procedure and the Green's-functions approach for the correlation problem. That the two methods are equivalent is seen, as follows. If we take the trial wave functions

$$|\Psi\rangle=\prod_{k<k_F}\left(\sum_{\alpha m} V_{\alpha m\sigma}(\vec{k})c^{\dagger}_{\vec{k}\alpha m\sigma}\right)\times\left(\sum_{\alpha m} V_{\alpha m-\sigma}(\vec{k})c^{\dagger}_{\vec{k}\alpha m-\sigma}\right)|0\rangle\,, \tag{3.37}$$

calculate the average $(\psi|H|\psi)$, and then minimize with respect to the $V_{\alpha m\sigma}(\vec{k})$, we find that they must be eigenvectors of the matrix $\underline{C}$ in (3.19) and satisfy the relation (3.31) for $\beta\to\infty(T=0)$. [This last condition follows immediately by direct evaluation of $\langle\psi|c^{\dagger}_{am\sigma}c_{an\sigma}|\psi\rangle$ using the Fourier transforms (3.6).] Hence, specifying a self-consistent set of occupation numbers is equivalent to a minimization procedure. The advantage of the Green's-function approach is as emphasized before, that we can take advantage of the atomic limit calculation to find the most stable ground-state configuration. In general, if the self-consistent ground state has some symmetry left, there are relations among the averages $\langle c^{\dagger}_{\alpha m\sigma}c_{\alpha n\sigma}\rangle$. Suppose for example that $|\psi)$ is invariant under C_3, so that $C_3|\psi)=|\psi)$. In such a case, remembering the transformation properties of the Wannier states, the relation

$$\langle\psi|c^{\dagger}_{\alpha m\sigma}c_{\alpha n\sigma}|\psi\rangle=\langle\psi|C_3^{-1}c^{\dagger}_{am\sigma}C_3C_3^{-1}c_{an\sigma}C_3|\psi\rangle \tag{3.38}$$

implies that

$$\langle c^{\dagger}_{\alpha 1\sigma}c_{\alpha 1\sigma}\rangle=\langle c^{\dagger}_{\alpha 2\sigma}c_{\alpha 2\sigma}\rangle$$

and (3.39)

$$\langle c^{\dagger}_{\alpha m\sigma}c_{\alpha n\sigma}\rangle=0 \text{ if } m\neq n\,.$$

The role of the off-diagonal $(m\neq n)$ averages, when they are different from zero, is best understood if we realize that in such a case it is always possible to introduce new basis Wannier states $d^{\dagger}_{\alpha m\sigma}=\sum_n a_{mn}c^{\dagger}_{\alpha n\sigma}$ for which $\langle d^{\dagger}_{\alpha m\sigma}d_{\alpha n\sigma}\rangle=0$ if $m\neq n$. So they serve actually to change the quantization basis. Hence, if we have reasons to suspect that the self-consistent solution has sizable off-diagonal averages [as for example all the solutions in I with $\theta_j=\frac{1}{4}\pi$ $(\frac{3}{4}\pi)$] we speed up the convergence procedure if we start right away from the correct averages. For instance, if we are looking for self-consistent solutions corresponding to the RO(2)-RS (real orbital order–real spin structure) atomic limit solution, where the orbitals

$$(1/\sqrt{2})[w_j^1(\vec{x})\pm w_j^2(\vec{x})]\equiv(1/\sqrt{2})(c^{\dagger}_{j1\sigma}\pm c^{\dagger}_{j2\sigma})|0\rangle\equiv|\psi^{\pm}\rangle \tag{3.40}$$

are occupied, we should start from input averages of the kind

$$\begin{aligned}
&\langle\psi^{+}|c^{\dagger}_{j1\sigma}c_{j1\sigma}|\psi^{+}\rangle=\langle\psi^{+}|c^{\dagger}_{j2\sigma}c_{j2\sigma}|\psi^{+}\rangle=\tfrac{1}{2}\,,\\
&\langle\psi^{+}|c^{\dagger}_{j1\sigma}c_{j2\sigma}|\psi^{+}\rangle=\tfrac{1}{2}\,,\\
&\langle\psi^{-}|c^{\dagger}_{1\sigma}c_{j1\sigma}|\psi^{-}\rangle=\langle\psi^{-}|c^{\dagger}_{j2\sigma}c_{j2\sigma}|\psi^{-}\rangle=\tfrac{1}{2}\,,\\
&\langle\psi^{-}|c^{\dagger}_{j1\sigma}c_{j2\sigma}|\psi^{-}\rangle=-\tfrac{1}{2}\,,
\end{aligned} \tag{3.41}$$

according to whether the occupied orbital at site j is ψ^{+} or ψ^{-}. Similarly, if we are looking for complex solutions, to estimate for instance the orbital contribution to the magnetic moment, we must use the appropriate off-diagonal average.

IV. RESULTS OF THE HF CALCULATIONS IN THE INSULATING PHASE FOR ONE ELECTRON IN A DOUBLY DEGENERATE BAND

Before presenting the results of the HF calculations with all the three states included (e_g and a_{1g}), we think it useful for illustrative purposes to discuss the case of one electron in a doubly degenerate e_g band in the corundum structure. In this way we can make a comparison between the HF results and the atomic limit calculations, get an understanding of the state of affairs in this simpler case which will serve us as a guideline for the more complete calculations, and finally assess the validity of the Chao-Gutzwiller[15] approach for the description of electron correlations in a doubly degenerate band.

Let us consider the Hamiltonian (3.11) for the case of two Wannier states of e_g symmetry, and take as orientative values $\mu=0.46$, $\alpha=0.29$, $\beta=0.0$, and $\nu=\pi=\delta=0.0$ eV. Again one can show that $U=U'+2J$ and we take $U=1.5$, $U'=1.3$, and $J=0.1$ eV. From now on the t_{2g} antibonding atomic level in (3.11), that is to say the terms t_{jj}^{mm}, will be set equal to zero.

A completely restricted HF calculation (that is to say all the occupation numbers $\langle n_{\alpha m\sigma}\rangle=\frac{1}{4}$ and the off-diagonal averages equal to zero) leads to a density-of-state curve of the kind shown in Fig. 2. The zero of the scale of the energy has been determined so that $\sum_{\lambda\vec{k}}\omega_{\lambda}(\vec{k})=0$ according to the convention of Ref. 15. In our notation it corresponds to 2.9 eV. Notice that the calculation reduces to a bare band-structure calculation, since the interaction matrix is, in such a case, proportional to the unit matrix, the proportionality constant being $\frac{1}{4}(U+2U'-J)=1$ eV. This solution is always a self-consistent solution in the sense that we obtain already at the first iteration the calculated output $\langle n_{\alpha m\sigma}\rangle=\frac{1}{4}$.

We can see that due to the degeneracy of the e_g orbitals in the trigonal symmetry, the Fermi level falls in a region of high density of states [$\rho(\epsilon_F)\simeq1.5$ states/eV spin V-atom)]. Hence from

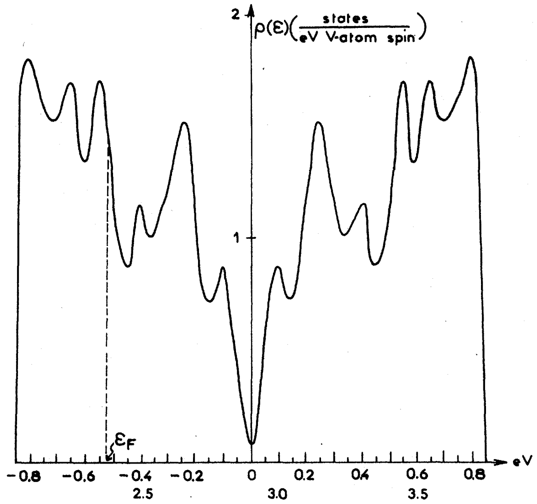

FIG. 2. Density of states for corundum structure with one electron per site in a doubly degenerate e_g band, without electron correlation.

the point of view of the Bloch-Wilson theory the system should be metallic. However a gap is found if one looks for the symmetry breaking solutions suggested by the atomic limit calculation in I. As an example, the density of states of the antiferromagnetic orbit–real spin structure AO(1)-RS state is depicted in Fig. 3. This is interesting in two respects: It shows, firstly, the possibility of opening a correlation gap of the Mott-Hubbard type in the e_g band and, secondly, that this occurs far away from the critical values of the ratios $-C_1/\bar{\epsilon}_p, -C_2/\bar{\epsilon}_p, -C_3/\bar{\epsilon}_p$, for which a transition from a metallic to an insulating state should occur according to ideas of Chao-Gutzwiller.[15] C_1, C_2, C_3 are equivalent to our quantities $U, U', U'-J$, and

$$\bar{\epsilon}_p = 2 \sum_{|\vec{k}|<k_F} \epsilon_{\vec{k}} \cdot$$

The conditions for criticality in this case of one electron in a doubly degenerate band are discussed in some detail in Appendix A, following Ref. 15 and imposing the constraint $C_1 - 3C_2 + 2C_3 = U - U' + 2J = 0$ appropriate for our case. Given our values for $U = 1.5, U' = 1.3, J = 0.1, -\epsilon_p = 0.65$(eV) as calculated from Fig. 2 and the critical ratios as derived from Fig. 11 of Appendix A, (minimum critical ratio $C_i/-\bar{\epsilon}_p \simeq 6$), we see that we are far away from criticality condition of Chao and Gutzwiller. As a consequence the application of the Gutzwiller theory by Brinkman and Rice[16] to the description of the correlated metallic state of V_2O_3 at low temperature under pressure becomes questionable. Indeed, in this theory, the mass enhancement factor is given by

$$m^*/m = [1 - (C_i/6\bar{\epsilon}_p)^2]^{-1}, \qquad (4.1)$$

taking that i for which one is nearest to criticality. However this expression when evaluated for the above set of values (actually in the metallic phase U should be somewhat less than 1.5 eV, the gap disappearing at 1.3 eV) gives a mass enhancement utterly insufficient to account for the observed ratio $m^*/m = \rho_{\text{eff}}(\epsilon_F)/\rho_b(\epsilon_F) \simeq 4$. $\rho_{\text{eff}}(\epsilon_F)$ we have estimated from the measured γ value at low temperature and high pressure[17] using the formula $\gamma = \frac{1}{3}\pi^2 N k_B^2 \rho_{\text{eff}}(\epsilon_F)$ and $\rho_b(\epsilon_F) = 1.5$ states/(eV

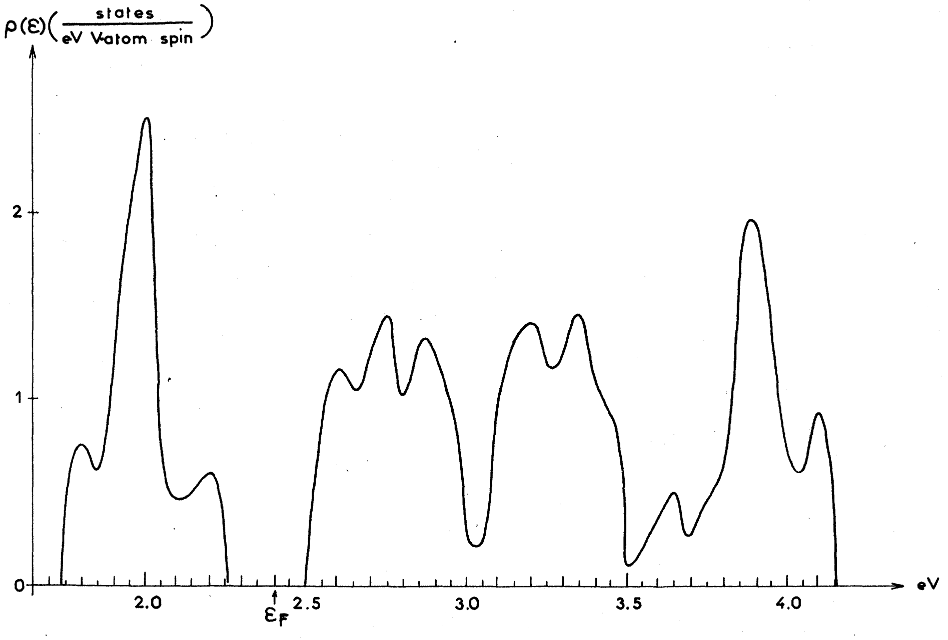

FIG. 3. Density of states for corundum structure with one electron per site in a doubly degenerate e_g band for the AO-RS configuration.

spin V-atom) is the bare density of the states as derived from Fig. 2. This latter value is close to the more realistic one of $1.0 \simeq 1.25$ obtained from the complete calculation including the a_{1g} which we shall discuss below; see also Ref. 5.

There is another interesting aspect relating the HF symmetry-breaking solutions and the corresponding ones found in the atomic limit calculations. Their ground-state energies E_G agree within 10%, provided $U/W \gtrsim 0.8$, where W is the bare bandwidth. So even near the Hubbard[18] condition for a metal insulator transition for a spherical Fermi surface ($U/W \simeq 0.8$, but actually this number should not be much model dependent, since we get a gap for about this value) we can fairly well estimate E_G from an unrestricted HF calculation by looking at the corresponding atomic limit calculation. This makes us confident in the validity of the procedure which we have followed, that is to say to describe the electron correlations starting from second-order perturbation theory even though this latter does not seem *a priori* applicable.

As a representative example we give in Table II the numerical values of E_G for the AO(1)-RS configuration and the AO(1)-FS configuration obtained with the two methods.

The expression for E_G in the atomic limit have been derived from Table V of I neglecting terms of the order $(J/U)^2$. In this way the broad features of the phase diagram in Fig. 7 of I turn out to be confirmed for the case of the HF calculations with two degenerate bands. The variation of E_G for various states of interest for later discussion and of $\Delta\epsilon_g$ the gap between the occupied and unoccupied states as a function of the Hubbard parameters U, U', J and the hopping integrals α, β, and μ are illustrated in Table III where all the numbers are in eV, E_G being expressed in eV/(molecule V_2O_3).

The labeling of the states is the same as that introduced in Table V of I except for the states PO-RS, PO-FS, and PO-PS which have no equivalent in the atomic limit. Indeed, PO indicates orbital paramagnetism, that is to say no phase correlations between orbital occupation of adjacent sites. Hence, for example, PO-RS represents a state with a real-spin correlation such that on each site $\langle n_{\alpha 1\sigma}\rangle = \langle n_{\alpha 2\sigma}\rangle$. Similarly PO-PS indicates the completely uncorrelated state for which $\langle n_{\alpha m\sigma}\rangle = \frac{1}{4}$. Its density of states at the Fermi level is $\rho(\epsilon_F) = 1.5$ states/(eV spin V-atom) for the first set of α, β, μ values as found above and $\rho(\epsilon_F) = 1.25$ states/(eV spin V-atom) for the second set of values. Also there is not much variation of $\rho(\epsilon_F)$ around $\simeq 1$ state/(eV spin V-atom) as a function of the parameters in Table III for the states AO(1)-FS and PO-FS when $\Delta\epsilon_g = 0$. In such a case the variation of $\rho(\epsilon_F)$ is discontinuous in the sense that one has either $\Delta\epsilon_g \neq 0$ or a high value for $\rho(\epsilon_F)$.

On the contrary, for the states PO-RS and AO(1)-RS $\rho(\epsilon_F)$ increases from zero continuosuly through the critical value U^c for which $\Delta\epsilon_g$ becomes zero when U is varied for a fixed set of α, β, μ and fixed ratio J/U'. This is a feature common to all the states having a spin structure which breaks the trigonal symmetry of the crystal. The reason is that the degeneracy at the Γ points of the two e_g bands arising from the e_g atomic states is lifted, since in a spin symmetry breaking structure RS the motion of the electron along the antiferromagnetic chains along the y axis (Fig. 3 of I) is different from that in the planes perpendicular to it, where all the spins are coupled ferromagnetically. Hence, it turns out to be possible to open a gap in the one-electron density of states of the Hubbard-Slater type for a certain ratio of U/W (usually of the order of 0.8) which disappears altogether with the disappearance of the spin ordering. One might think that the same would happen for a state like RO(1)-PS, that is to say a state without spin ordering but nonetheless breaking the trigonal symmetry, through the RO(1) orbital ordering. However, for $0.1 < J/U' < 0.2$ and $0.8 < U/W < 1.0$, we were not able to find such a self-consistent solution. Starting from a configuration such as RO(1)-PS through an appropriate set of occupation numbers, the HF self-consistent solution always converged to the uncorrelated spin and orbit paramagnetic state PO-PS.

For the set of parameters given in Table III, we are well inside the stability region of the AO(1)-RS configuration in the phase diagram of Fig. 7 of I. Accordingly we find that the AO(1)-RS states have

TABLE II. Comparison of the ground-state energies for the AO(1)–RS and AO–FS state obtained by an Hartree-Fock and an atomic limit calculation.

Configuration	E_G (HF calculation)	E_G (atomic-limit calculation)
AO(1)–RS	−0.538 eV/molecule V_2O_3	$-\frac{1}{U'-J}(3\alpha^2+2\mu^2)+\frac{7}{2}\alpha^2\frac{J}{U^2}=-\frac{0.550\text{ eV}}{\text{molecule } V_2O_3}$
AO(1)–FS	−0.482 eV/molecule V_2O_3	$-\frac{1}{U'-J}(\frac{9}{4}\alpha^2+2\mu^2)=-0.510\frac{\text{eV}}{\text{molecule } V_2O_3}$

TABLE III. Illustration of the variation of the ground-state energies and gaps in the density of states for several ground-state configurations as a function of the hopping integrals α, β, μ, and Hubbard parameters. The system considered corresponds to one electron in a doubly degenerate e_g band.

	$\alpha=0.29,\ \beta=0.0,\ \mu=0.46$						$\alpha=0.29,\ \beta=0.1,\ \mu=0.46$			
	$U=1.4, U'=1.2, J=0.1$		$U=1.5, U'=1.3, J=0.1$		$U=1.5, U'=1.1, J=0.2$		$U=1.5, U'=1.3, J=0.1$		$U=1.45, U'=1.25, J=0.1$	
	E_G	$\Delta\epsilon_g$	E_G	$\Delta\epsilon_g$	E_G	$\Delta\epsilon_g$	E_G	$\Delta\epsilon_g$	E_G	ϵ_g
AO(1)–RS	−0.583	0.10	−0.538	0.25	−0.662	0.10	−0.558	0.25	−0.580	0.20
PO– RS	−0.577	0.00	−0.519	0.05	−0.662	0.10	−0.537	0.00	−0.566	0.00
AO(1)–FS	−0.521	0.00	−0.482	0.10	−0.612	0.00	−0.512	0.00	−0.531	0.00
PO– FS	−0.528	0.00	−0.465	0.00	−0.612	0.00	−0.514	0.00	−0.532	0.00
PO– PS	−0.546	0.00	−0.471	0.00	−0.596	0.00	−0.487	0.00	−0.524	0.00

the lowest energy and are far below all the other spin configurations in the phase diagrams [of the order of 0.05 Ev/(molecule V_2O_3)]. It is worth noticing however that the states PO-RS are always much closer to the ground state than all the others. This feature is independent of the actual values for $\alpha, \beta, \mu, U, U', J$, provided one is inside the stability region of the AO(1)-RS configuration. We shall return to this point in paper III,[19] (hereafter, III).

Concerning the properties of the ground-state AO(1)-RS, it is interesting to look at the kind of HF self-consistent set of occupation numbers we obtain. This set is given in Table IV and corresponds to the set of parameters in the second column of Table III [see Fig. 8(a) of I for the corresponding atomic limit occupancy]. Here the index α numbers the V atoms in the unit cell according to Fig. 3 of I. The occupation numbers for the sites $\alpha=3, 4, 5, 7$ can be easily obtained by continuing throughout the lattice the AO(1)-RS configuration. The convergence was achieved up to the fifth decimal in all the calculations of Table III. The interesting feature to be noticed is that although we started from an input configuration of one electron per site in self-consistency, we found

$$\sum_{m\sigma}\langle n_{1m\sigma}\rangle = 1.008\,, \quad \sum_{m\sigma}\langle n_{2m\sigma}\rangle = 0.992\,.$$

Indicating by Δc the deviation from 1, the average number of electrons per site in our problem, so that a positive (negative) value of Δc indicates excess (defect) of charge relative to 1, we can easily draw Fig. 4 based on Table IV where a plus sign indicates an excess and a minus sign a defect of charge. Considering Δc as an order parameter, we see that the order is completely antiferromagnetic in the sense that an excess of charge on a site is accompanied by a defect on the four immediate neighbors. In other words, an AO(1)-RS self-consistent solution exists with a charge density wave of the kind shown in Fig. 4. [This feature is common to all the self-consistent

TABLE IV. Self-consistently determined HF occupation numbers for the e_g electrons on the sites 1, 2, 6, and 8 in the rhombohedral unit cell.

	$\alpha=1$	$\alpha=2$	$\alpha=6$	$\alpha=8$
$\langle n_{\alpha 1}\uparrow\rangle$	0.745	0.221	0.020	0.016
$\langle n_{\alpha 2}\uparrow\rangle$	0.183	0.721	0.060	0.034
$\langle n_{\alpha 1}\downarrow\rangle$	0.020	0.016	0.745	0.021
$\langle n_{\alpha 2}\downarrow\rangle$	0.060	0.034	0.183	0.721

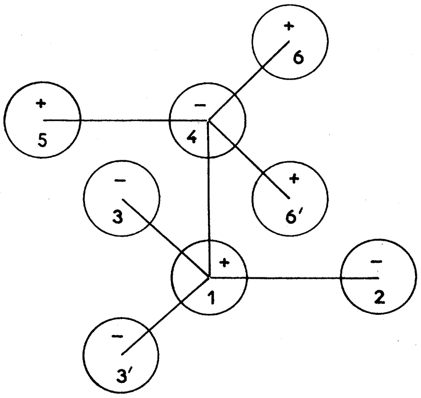

FIG. 4. Distribution of the excess (+) and defect (−) charge Δc throughout the corundum lattice for an AO-RS self-consistent solution. Regarding Δc as an order parameter, the order is completely antiferromagnetic.

HF solutions corresponding to the solutions is the argument 1 of Table V of I. It is absent in the solutions with argument 2 and those with orbital paramagnetism, e.g., PO-RS and PO-FS.] Hence, one expects a distortion of the lattice tending to shorten the distance of the vertical pairs, contrary to what is experimentally observed (Ref. 5 of I). However, there is another source of distortion in the lattice which must be taken into account if one wants to explain the experimental findings (Ref. 5 of I). This second distortion mechanism is magnetostrictive in origin and takes place merely due to the existence of a magnetic structure lacking the trigonal symmetry of the lattice. For this effect, the presence of the a_{1g} electrons is essential as will be shown in a moment. Briefly, what happens is that through intra-atomic exchange the e_g electrons polarize in part the a_{1g} electrons. For the pairs ferromagnetically coupled, this means that a triplet component is introduced in the molecular-orbital wave function for the a_{1g} electrons leading to a loss in bonding energy more than compensated for by the gain in intra-atomic exchange energy due to the resulting partial localizations of the a_{1g} electrons. (Remember to this purpose that the a_{1g} Wannier states are not degenerate so that the ground-state molecular wave function is a spin singlet; hence lowering of the kinetic energy can take place only in this spin configuration. In a triplet, spin configuration electrons cannot jump from one site to the other of the molecule due to the Pauli principle). As a reaction to the weakening of the electronic bond the atoms constituting the pair increase their distance as much as the oxygen cage around them allows. Nothing of the sort happens for the pairs where the coupling between e_g electrons is antiferromagnetic. In such a case, in fact, there is only a slowing down of the flipping rate of the two-spin configurations constituting the spin singlet of the a_{1g} molecular function without any dramatic change in the internuclear distance. A very sketchy model for the above state of affairs is the following: Suppose we are considering the vertical pair in the metallic state with two electrons per site. Then the total ground-state energy electronic binding plus internuclear repulsion plus lattice energy can be written as

$$4t_0+\tfrac{1}{2}[U-(U^2+16\rho^2)^{1/2}]+\tfrac{1}{2}\sum_j \alpha_j^2[C_j-(C_j^2+16\mu^2)^{1/2}] + Z_{\text{eff}}^2\frac{e^2}{R_m}-\alpha_M\frac{e^2}{R_m}, \qquad (4.2)$$

t_0 being the atomic level.

Here we have indicated by ρ the hopping integral of the a_{1g} electron, by μ the one of the e_g electrons and neglected the interaction between them. The energy for the e_g molecular state has been taken to be a mixture of the low-lying configurations given in Sec. III of I; accordingly the C_j's represent the quantities $U'-J$, $U'+J$, $U+J$ with the condition that $\sum \alpha_j^2=1$. Notice that in an isolated molecule, there would be no mixture of such states. However, as a result of the interactions with the medium, one expects a certain amount of mixing since some quantum numbers are not conserved anymore. The third term in Eq. (4.2) is the internuclear repulsion of the two nuclei of the molecule with an effective unscreened charge Z_{eff} at a distance R_m along the vertical axis (by symmetry the distortion is along the z axis). Finally we have schematized the effect of the lattice by a Madelung potential $-\alpha_M e^2/R_m$. This is a very crude approximation, although the exact form of this interaction is not relevant to the kind of argument we have in mind.

By assuming an exponential dependence of the hopping integrals on the internuclear distance so that $\rho=\rho_0 e^{-aR_m}$ and $\mu=\mu_0 e^{-aR_m}$, the equilibrium position of the nuclei in the metallic phase is determined by the equation

$$\frac{8a\rho^2}{(U^2+16\rho^2)^{1/2}}+\sum_j \alpha_j^2\frac{8a\mu^2}{(C_j^2+16\mu^2)^{1/2}} - (Z_{\text{eff}}^2-\alpha_M)\frac{e^2}{R_m^2}=0. \qquad (4.3)$$

In the antiferromagnetic phase the e_g electrons become polarized so that $\alpha_j=0$ except for that j for which $C_j=U'-J$. Allowing for a partial exchange polarization of the a_{1g} electrons, we may write the ground-state energy for this case as

$$4t_0+(1-b^2)\tfrac{1}{2}[U-(U^2+16\rho^2)]^{1/2}+b^2 2J$$
$$+\tfrac{1}{2}\{U'-J-[(U'-J)^2+16\mu^2]\}^{1/2}+(Z_{\text{eff}}^2-\alpha_M)(e^2/R). \qquad (4.4)$$

The new equilibrium position R_a is now determined by the equation

$$(1-b^2)\frac{8a\rho^2}{(U^2+16\rho^2)^{1/2}}+\frac{8a\mu^2}{[(U'-J)^2+16\mu^2]^{1/2}}$$
$$-(Z_{\text{eff}}-\alpha_M)(e^2/R_a^2)=0. \qquad (4.5)$$

If we now evaluate the left-hand side of this equation at $R=R_m$, we see that it is negative if we realistically assume $J/U\simeq 0.1$, $b^2\simeq 0.2$, and $\rho^2 \gtrsim 2\mu^2$ [see Eqs. (2.16) and (2.17) for this last inequality]. Hence $R_a > R_m$ as observed experimentally (Ref. 5, I). The same argument holds true for the pair of V atoms ferromagnetically coupled in the basal plane. The resulting distortion can be viewed as a rotation of the pairs in the $\vec{a}_M-\vec{c}_M$ plane (Fig. 3, I), that is to say the plane determined by the ferromagnetic bonds. Obviously there is a threefold degeneracy in the choice of the direction of the ferromagnetic bond in the basal plane, accounting for the twinning of the crystal after the distortion (Ref. 5, I).

In our opinion, the above polarization and consequent localization of the a_{1g} states is the primary and most effective source of distortion of the lattice at the metal–antiferromagnetic insulator phase transition. Once this distortion is set up, the charge-density distribution depicted in Fig. 4, if it represents a real physical effect at all, tends to stabilize the increase in the internuclear distance for the pair in the basal plane (direction $\vec{R}_1-\vec{R}_2$ in Fig. 3 of I) and to hinder the similar distortion for the vertical pair. This is in keeping with the experimental finding showing an increase of $\simeq$1.5% for the vertical pair compared with the $\simeq$3.5% increase for the pair in the basal plane (Ref. 5, I). However, the different behavior of the two pairs might also be explained by observing that the polarization of the a_{1g} electrons in the vertical pair is much more difficult than in the pair in the basal plane since $|\rho| \gg |\sigma|$, σ being the hopping integrals for a_{1g} electrons in the basal plane [see Eqs. (2.16) and (2.17)].

The above considerations also allow a straightforward interpretation of the variation of the c/a ratio in transition metal oxides of corundum structure as illustrated in Fig. 5. The key idea is that a bond between V atoms along the vertical pairs is not only a bond between these two particular atoms but it actually involves the two oxygen octahedra which surround them sharing a face. This is because the effective transfer integral between magnetic electrons contains a contribution from the ligands [Eq. (2.16)]. Hence a strong bond between electrons in the vertical pairs also entails a strong bond of three successive layers of oxygen atoms, so that the oxygen cage shrinks in the c direction and expands in the direction orthogonal to it (a axis). As a consequence, the c/a ratio becomes smaller. If the vertical bond is loose, the c/a ratio will have to increase. This explains why its value is maximum in V_2O_3 among transition-metal compounds of corundum structure.[20]

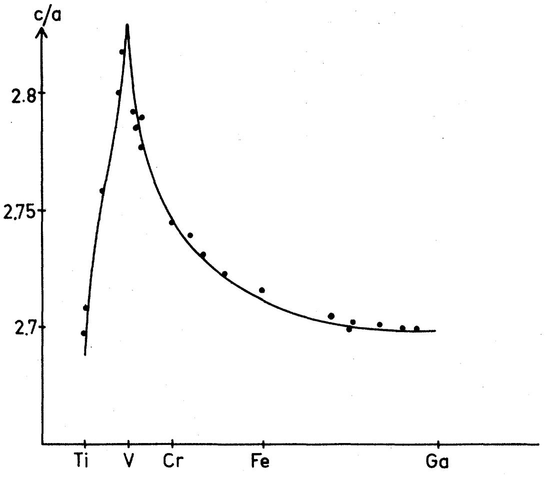

FIG. 5. c/a ratio of various transition-metal oxides.

Notice that a breaking of the trigonal crystal symmetry (that is to say a distortion in the basal plane) is not at all necessary to obtain a gap in the one-electron density of the states. Indeed the crystal symmetry of the Hamiltonian we started from, Eq. (3.11), is that of the trigonal phase of V_2O_3. This trigonal symmetry is broken and reduced to monoclinic by the spin ordering which allows a gap to be opened in the density of states and at the same time induces a lattice distortion through the mechanism illustrated above.

Another point deserving discussion is the one concerning the magnetic moment. From Table IV one derives for the number of Bohr magnetons per site the following values:

$$\sum_{m\sigma}(-1)^\sigma\langle n_{1m\sigma}\rangle=0.848, \quad \sum_{m\sigma}(-1)^\sigma\langle n_{2m\sigma}\rangle=0.892,$$
$$\sum_{m\sigma}(-1)^\sigma\langle n_{6m\sigma}\rangle=-0.848, \quad \sum_{m\sigma}(-1)^\sigma\langle n_{8m\sigma}\rangle=-0.892. \qquad (4.6)$$

The fact that a slightly different number of Bohr magnetons per site is found for adjacent pairs ferromagnetically coupled is a consequence of the existence of the charge-density wave. Neglecting this difference, one would be led to say that on the average around 0.87-Bohr magnetons per site are present.

However, we must keep in mind that $n_{\alpha m \sigma}$ represents an occupation number for electrons in a wave function of the type shown in Eq. (1.1) since we have adopted a molecular-orbital picture to eliminate the effect of the oxygens on the magnetic electrons. Hence the above number of Bohr magnetons is spread out over the whole cluster of six oxygens surrounding each V atom. As a result only the fraction $1-\lambda_\pi^2$ is left on this latter.[21] The fraction λ_π^2 of magnetic moment on the oxygens is not compensated for as in other antiferromagnetic systems[21] where each oxygen atom is surrounded by as many transition metal atoms of spin-up as of spin-down. In the case of V_2O_3 there are four V atom neighbors to each oxygen atom, three of them being spin-polarized opposite to the fourth. This suggests that in the antiferromagnetic insulating phase of V_2O_3 the ligands are not diamagnetic each one carrying a fraction of magnetic moment given by $\frac{1}{6}2\lambda_\pi^2=\frac{1}{3}\lambda_\pi^2$. The factor $\frac{1}{6}$ is due to the six neighboring oxygens which surround a V site. Hence for half a formula unity $VO_{1.5}$ the magnetic moment is given by

$$\langle\mu\rangle=[1-\lambda_\pi^2+(1.5)\tfrac{1}{3}\lambda_\pi^2]\langle n\rangle=\langle n\rangle(1-\tfrac{1}{2}\lambda_\pi^2)\,, \qquad (4.7)$$

where $\langle n\rangle$ is the number of magnetons per site as found from the HF self-consistent calculations. As already shown $\langle n\rangle$ turns out to be of the order of $0.85 \simeq 0.90$. In the framework of the approach taken to describe the magnetic electrons in V_2O_3, it is the quantity in Eq. (4.7) that should be compared with the experimental findings (Ref. 4, I). Notice that in this last reference, the observed moment per V atom $[(1.2\pm 0.1)\mu_B]$ is actually all attributed to the transition-metal atom only. According to the above argument, the observed magnetic moment should be attributed to the two constituents of the formula unit V_2O_3 in the proportion $\frac{1}{2}\lambda_\pi^2/(1-\lambda_\pi^2)$. By taking a reasonable value for $\lambda_\pi^2(\simeq 0.3)$ as derived below, the calculated moment per half formula unit ranges between 0.73 and 0.76 μ_B far away from the observed value.

This calculated moment per site for one electron in a doubly degenerate band would seem to support the view that two magnetic electrons are present in V_2O_3, each one contributing a reduced magnetic moment of about (0.8–0.9) μ_B because of itinerancy and further reduced by the factor $(1-\frac{1}{2}\lambda_\pi^2)$ because of covalency.

However, apart from the fact that in such a case the magnetic moment would turn out to be far too big ($\simeq 1.4\mu_B$) compared to the experimental value and putting aside the consideration of Sec. V which would tend to still raise its value, we think that this is not the correct explanation in the light of the following findings. Indeed, as discussed at length below, the inclusion of one a_{1g} electron in our self-consistent unrestricted Hartree-Fock calculation results in the following situation: For $J/U' < 0.15$ an AO(1)-RS structure for the e_g electrons and a diamagnetic a_{1g} band is found to be the most stable (lowest ground-state energy) among a large number of possible self-consistent structures which we tried. A gap is present and the amount of intra-atomic exchange polarization of the a_{1g} electrons caused by the e_g electrons is of the order of 0.1 electrons per site (this means that on the average 0.1 more magnetic electrons are found in the e_g band in presence of the a_{1g} band than in its absence). This is mainly due to the fact that the hopping integral ρ for the a_{1g} electrons along the vertical direction is by far the biggest (in absolute value) among all the others—a factor of 2 or more times the next biggest hopping integral μ; see expressions in (2.16) and (2.17). This high value of ρ is brought about by the fact that the lobes of the a_{1g}-$3d$ functions point toward the z axis and the fact that there is a constructive interference between the bare $(3d, 3d)$ hopping integral and the covalency contribution to it. As a result, the most stable energetic configuration for the a_{1g} electrons is a diamagnetic molecular-orbital level for the vertical pair, enlarged to a band by interactions between pairs. Only those a_{1g} electrons within roughly $2J$ of the Fermi level in the metallic state are involved in the intra-atomic exchange polarization since for them the kinetic energy increases because of localization is more than compensated for by the gain in intra-atomic exchange energy. Since their density of states at the Fermi level is low (Fig. 7) a small fraction of a_{1g} electrons is involved in the process. Moreover, a gap in the a_{1g} density of states is easily opened following the opening of the gap in the e_g density of states due to the onset of the magnetic order. However, the total magnetic moment per site in this case ($\simeq 1.0\mu_B$ times 0.85 the covalency reduction factor) is insufficient to explain the experimental finding.

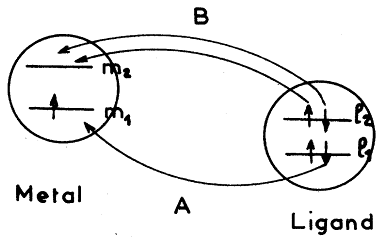

FIG. 6. Diagram showing schematically two possible transfer processes A, B between the magnetic ion M and the diamagnetic surroundings in the configuration-interaction picture.

V. MAGNETIC MOMENT IN V$_2$O$_3$

We shall try in the following to propose a mechanism which permits us to find better agreement with the experiment. As a matter of fact the point of view adopted above in assessing and incorporating the effect of the oxygen lattice on the magnetic electrons of the V atom is based on the molecular orbital picture. According to this picture, the ground-state wave function for a cluster of a metal ion plus the surrounding oxygen octahedron is described by the Slater determinant

$$\psi_G' = \frac{1}{\sqrt{3\,!}} \left\{ \frac{m_1 - \lambda e_l}{[1 - 2\lambda\,\langle m_1 | l_1\rangle + \lambda^2]^{1/2}} \uparrow, \frac{l_1 + \gamma m_1}{[1 - 2\gamma\langle m_1 | l_1\rangle + \gamma^2]^{1/2}} \uparrow, \frac{l_1 + \gamma m_1}{[1 - 2\gamma\langle m_1 | l_1\rangle + \gamma^2]^{1/2}} \downarrow \right\}$$

$$(\lambda = \gamma + \langle m_1 | l_1\rangle) \tag{5.1}$$

for the schematic case illustrated in Fig. 6 in which there is only one occupied orbital on the metal ion and one occupied level on the ligand (generalization is straightforward). The determinant (5.1) forms the essence of the molecular-orbital description of covalency and it is completely equivalent to the ground-state wave function built on the basis of the Heitler-London model with configuration interaction.[22] In this last picture, the ground state ψ_G' is written as

$$\psi_G' = N(\psi_G + \gamma\psi_E), \tag{5.2}$$

where ψ_G is the purely ionic state described by the Slater determinant

$$\psi_G = \frac{1}{\sqrt{3\,!}} \left\{ \frac{m_1 - \langle m_1 | l_1\rangle\, l_1}{[1 - \langle m_1 | l_1\rangle^2]^{1/2}} \uparrow, l_1 \uparrow, l_1 \downarrow \right\}, \tag{5.3}$$

and ψ_E is the excited (charge-transfer) configuration

$$\psi_E = \frac{1}{\sqrt{3\,!}} \left\{ \frac{m_1 - \langle m_1 | l_1\rangle\, l_1}{[1 - \langle m_1 | l_1\rangle^2]^{1/2}} \uparrow, l_1 \uparrow, m_1 \downarrow \right\} \tag{5.4}$$

where process A in Fig. 6 has taken place, i.e., the ligand to metal half-filled orbital transfer. A variational calculation shows that to lowest order in γ one finds

$$\gamma = \frac{\langle\psi_G | \psi_E\rangle\langle\psi_G | H | \psi_G\rangle - \langle\psi_G | H | \psi_E\rangle}{\langle\psi_E | H | \psi_E\rangle - \langle\psi_G | H | \psi_G\rangle}, \tag{5.5}$$

where H is the many-body Hamiltonian.

The advantage of writing ψ_G' in (5.2) as the Slater determinant (5.1) is that all the magnetic properties of the cluster can be described in a one-electron picture, using the antibonding orbital

$$\phi = (m_1 - \lambda l_1)/[1 - 2\lambda\langle m_1 | l_1\rangle + \lambda^2]^{1/2}.$$

In fact this is what we have done in Sec. I when constructing the one-electron states for the magnetic electrons. However, one must bear in mind that the molecular-orbital picture and the configuration interaction method are only equivalent ways of describing covalency if other kinds of processes are negligible or cannot take place. Indeed, one must recognize that the configuration interaction method allows for a wealth of processes which cannot be adequately described in the framework of a one-electron picture. One of these, which is important for our purposes is the ligand-to-metal-empty-orbitals electron transfer depicted in Fig. 6 in process B. Such a process can affect the total spin distribution of the cluster as described by the molecular orbital picture; indeed, it is well known[22] to produce a negative spin density on the ligands (spin polarization opposite to that of the metal ion) and consequently a positive spin polarization on the metal ion, both of which add to the spin-density distribution as determined by the process A (Fig. 6) described above, Eq. (5.2). For convenience we repeat the derivation of Ref. 22, and as there we consider here a simple three-electron system unperturbed ground state (Fig. 6).

$$\psi_G = (1/\sqrt{3\,!})\{m_1\uparrow, l_2\uparrow, l_2\downarrow\}, \tag{5.6}$$

where m_1 is the magnetic orbital, such as $t_{2g}(\pi)$ in V$_2$O$_3$ and l_2 is the molecular ligand orbital belonging to the same representation as the empty orbital of the metal m_2 which we assume of σ symmetry. Hence $\langle m_1 | l_2\rangle = 0$. The two excited states differing by the spin of the transferred electron are given by

$$\psi_{E_a} = (1/\sqrt{3\,!})\{m_1\uparrow, m_2\uparrow, l_2\downarrow\}, \tag{5.7}$$

$$\psi_{E_b} = (1/\sqrt{3\,!})\{m_1\uparrow, l_2\uparrow, m_2\downarrow\}. \tag{5.8}$$

It should be emphasized that the excited orbital m_2 in (5.7) actually differs from that in (5.8) because of the exchange interaction with $m_1\uparrow$. This difference is not important for our purposes although it might be in the case when m_2 represents a 4s orbital and one is interested in hyperfine effects on the metal atom.

The perturbed ground-state wave function can now be written as

$$\psi_G' = N(\psi_G + \gamma_a\psi_{E_a} + \gamma_b\psi_{E_b}). \tag{5.9}$$

The transfer parameters may be calculated using expressions (5.5). The exchange integral J between m_1 and m_2 makes the energy of ψ_{E_a} smaller than that of ψ_{E_b}. Referring again to expression (5.5) we can write

$$\gamma_a = b/(\Delta E - J), \quad \gamma_b = b/\Delta E, \tag{5.10}$$

where b refers to the numerator and ΔE to the denominator in (5.5). The exchange integral J is positive and hence $|\gamma_a| > |\gamma_b|$. This produces a negative unpaired spin density on the ligand and a consequently positive spin density on the metal which can be calculated by rewriting (5.9) as

$$\psi'_G = \frac{1}{\sqrt{3\,!}}\left\{m_1\uparrow, \frac{l_2+\gamma_a m_2}{[1+2\gamma_a\langle m_2|l_2\rangle+\gamma_a^2]^{1/2}}\uparrow, \frac{l_2+\gamma_b m_2}{[1+2\gamma_b\langle m_2|l_2\rangle+\gamma_b^2]^{1/2}}\downarrow\right\}. \qquad (5.11)$$

Determinant (5.11) differs from (5.9) by the presence of small cross products proportional to $\gamma_a\gamma_b$ which can be neglected. Notice that expression (5.11) is still valid even for the case $S=\langle m_2|l_2\rangle \neq 0$ if terms in S^2 are neglected. Moreover had we inserted from the outset the occupied ligand orbital l_1 belonging to the same representation as m_1 in the wave function (5.6) we would have arrived at the ground state

$$\psi'_G = \frac{1}{\sqrt{5\,!}}\left\{\frac{m_1-\lambda l_1}{[1-2\lambda\langle m_1|l_1\rangle+\lambda^2]^{1/2}}\uparrow, \frac{l_1+\gamma m_1}{[1-2\gamma\langle m_1|l_1\rangle+\gamma^2]^{1/2}}\uparrow, \frac{l_1+\gamma m_1}{[1-2\gamma\langle m_1|l_1\rangle+\gamma^2]^{1/2}}\downarrow, \frac{l_2+\gamma_a m_2}{[1+2\gamma_a\langle m_2|l_2\rangle+\gamma_a^2]^{1/2}}\uparrow, \frac{l_2+\gamma_b m_2}{[1+2\gamma_b\langle m_2|l_2\rangle+\gamma_b^2]^{1/2}}\downarrow\right\}, \qquad (5.12)$$

which is a straightforward generalization of (5.11) and more useful for our further discussion. Since the orbitals (5.12) are mutually orthogonal, the total spin density is simply a sum of the one-electron contributions so that to second order in λ^2 or $\lambda\langle m|l\rangle$ we find

$$\begin{aligned}\rho_\uparrow-\rho_\downarrow &= m_1^2(1-\lambda^2)-2\lambda m_1 l_1+2\lambda\langle m_1|l_1\rangle m_1^2+\lambda^2 l_1^2\\ &\quad+\{[\gamma_a+\langle m_2|l_2\rangle]^2-[\gamma_b+\langle m_2|l_2\rangle]^2\}m_2^2\\ &\quad+[\gamma_b^2+2\gamma_b\langle m_2|l_2\rangle-\gamma_a^2-2\gamma_a\langle m_2|l_2\rangle]\,l_2^2\,.\end{aligned} \qquad (5.13)$$

The total moment seen by neutrons is just the integral of (5.13). Hence the moment per metal ion and per magnetic orbital occupied is given by

$$\mu_M = 1-\lambda^2+(2J/\Delta E)[\gamma_b^2+\gamma_b\langle m_2|l_2\rangle], \qquad (5.14)$$

whereas the moment on one oxygen atom (in an antiferromagnetic structure) would be

$$\mu_L = \{\lambda^2-(2J/\Delta E)[\gamma_b^2+\gamma_b\langle m_2|l_2\rangle]\}(N_{M\uparrow}-N_{M\downarrow})/N_L\,, \qquad (5.15)$$

where we have indicated by $N_{M\sigma}$ the number of metal nearest neighbors of a ligand of spin σ and by N_L the number of oxygen atoms around a metal ion. Also in deriving Eqs. (5.14) and (5.15) we have expanded γ_a in powers of J/Δ_E (usually <0.2) writing $\gamma_a=\gamma_b(1+J/\Delta_E)$. The generalization of the case of V_2O_3 is immediate. Since the a_{1g} electrons are engaged in a more or less covalent bond in the vertical pairs, they are nonmagnetic except for an intra-atomic exchange partial polarization already mentioned above. Hence only one magnetic electron is left on the V atom in an $e_g(\pi)$ state [that is to say a $t_{2g}(\pi)$ state neglecting any deviation from ideal octahedral configuration]. There remains an empty $e_g(\pi)$ state nearly degenerate with the one occupied (remember that the trigonal degeneracy is lifted in the antiferromagnetic phase because of the spin arrangement; this is important for our purposes since it means that the ground state is an orbital singlet and that the wave function of the cluster can be expressed by a single Slater determinant) and two empty $E_g(\sigma)$ states on the metal ion. As a result the moment on this latter is given by

$$\begin{aligned}\mu_M &= 1-\lambda_\pi^2+2(2J/\Delta E)[\gamma_\sigma^2+\gamma_\sigma\langle\phi_\sigma^{3d}|\chi_{2p\sigma}\rangle]\\ &\quad+(2J/\Delta E)[\gamma_\pi^2+\gamma_\pi\langle\phi_\pi^{3d}|\chi_{2p\pi}\rangle]\\ &\quad+2(2J/\Delta E)[\gamma_{\sigma s}^2+\gamma_{\sigma s}\langle\phi_\sigma^{3d}|\chi_{2s\sigma}\rangle],\end{aligned} \qquad (5.16)$$

since there are two occupied ligand orbitals of σ symmetry which can make transitions to the empty metal orbital of the same symmetry and one ligand orbital of π symmetry allowing a jump on the only empty metal orbital of the same symmetry. Similarly

$$\mu_L = (1-\mu_M)(N_{M\uparrow}-N_{M\downarrow})/N_L\,, \qquad (5.17)$$

where μ_M is taken from (5.16).

Now, in order to calculate the reduced moment (5.16) on the metal ion we need to know the quantities γ_σ, γ_π, $\gamma_{\sigma s}$, ΔE, and J. The expression for the covalency parameter γ is given in Eq. (5.5) as a function of $\Delta E=(\psi_E|H|\psi_E)-(\psi_G|H|\psi_G)$. A reliable approximation to this last quantity can be obtained by looking at the photoemission and x-ray emission and adsorption spectra in V_2O_3.[4] We derive, using Fisher's notations in Ref. 4,

$$\begin{aligned}&\Delta E(1t_{2g}\to 2t_{2g}\rangle \simeq 3.5\ \text{eV}\,,\\ &\Delta E(2e_g\to 3e_g)\simeq 9\ \text{eV}\,,\\ &\Delta E(1e_g\to 3e_g)\simeq 22\ \text{eV}\end{aligned} \qquad (5.18)$$

where $1t_{2g}$ ($2t_{2g}$) represent the bonding (antibonding) molecular orbital of $t_{2g}(\pi)$ symmetry, $2e_g$ ($3e_g$) the bonding (antibonding) molecular orbital of $e_g(\sigma)$ symmetry and $1e_g$ the bonding molecular orbital of $e_g(\sigma)$ symmetry of mainly $2s$ character. In this way, polarization effects are automatically taken into account (see Sec. 3.1.2 of Ref. 22, p. 544). Unfortunately we are not in the same favorable position when evaluating the matrix elements in Eq. (5.5). In the lack of many electron calculations for these matrix elements we must resort to the one-electron analogy, that is to say replace the expression in the numerator of (5.5) by the following:

$$-\frac{\langle\chi|H_0|\phi\rangle}{\langle\chi|\phi\rangle\langle\chi|H_0|\chi\rangle}\,, \tag{5.19}$$

where again H_0 represents an effective one-electron Hamiltonian as in Sec. I and χ and ϕ represent one-electron orbitals for ligand and metal ion, respectively. This approximation should not be too bad since the main effects of polarization of the electron cloud is in the denomination of Eq. (5.5).

There is still another problem to face for the calculations of the matrix elements appearing in (5.19). These latter have been evaluated by Ashkenazi and Chuchem[5] in the trigonal metallic phase. However, these authors use a muffin-tin potential so that the crystal potential in H_0 is split into a position-dependent part V_{ins} inside the muffin-tin spheres and a constant part V_{out} outside the spheres; moreover Table II in their paper provides only the matrix elements $\langle\chi|V_{\text{ins}}|\phi\rangle$. If we write (5.19) as

$$\begin{aligned}\langle\chi|H_0|\phi\rangle+\langle\chi|\phi\rangle[\langle\phi|H_0|\phi\rangle-\langle\chi|H_0|\chi\rangle]-\langle\chi|\phi\rangle\langle\phi|H_0|\phi\rangle\\ =\langle\chi|V_{\text{ins}}|\phi\rangle+\langle\chi|\phi\rangle\Delta E+\langle\chi|T+V_{\text{out}}|\phi\rangle\\ -\langle\chi|\phi\rangle\langle\phi|T+V_{\text{out}}+V_{\text{ins}}|\phi\rangle\,. \end{aligned}\tag{5.20}$$

We estimate that the last two terms of the right-hand side of this expression nearly cancel. Hence, we use the following formulas to evaluate the various γ's we need:

$$\begin{aligned}\gamma_\pi&=-[\langle\chi_{2p\pi}|V_{\text{ins}}|\phi^{3d}_{t2g}\rangle+\langle\chi_{2p\pi}|\phi^{3d}_{t2g}\rangle\Delta E]/\Delta E\,,\\ \gamma_\sigma&=-[\langle\chi_{2p\sigma}|V_{\text{ins}}|\phi^{3d}_{Eg}\rangle+\langle\chi_{2p\sigma}|\phi^{3d}_{Eg}\rangle\Delta E]/\Delta E\,,\\ \gamma_{\sigma s}&=-[\langle\chi_{2s\sigma}|V_{\text{ins}}|\phi^{3d}_{Eg}\rangle+\langle\chi_{2s\sigma}|\phi^{3d}_{Eg}\rangle\Delta E]/\Delta E\,,\end{aligned}\tag{5.21}$$

together with relation (2.5). Although the transfer and overlap matrix elements of Table II in Ref. 5 are calculated for the metallic state, they should not be too different in the insulating phase. Moreover we take in Table II, the higher values for the matrix elements to account for the orbital expansion of the $3d$ wave function in the excited state. The numerical results are as follows (S indicating the overlap integral):

$$\begin{aligned}\gamma_\pi&=0.40\rightarrow\lambda_\pi=\gamma_\pi+S_\pi=0.55\,,\\ \gamma_\sigma&=-0.50\rightarrow\lambda_\sigma=\gamma_\sigma+S_\sigma=-0.72\,,\\ \gamma_{\sigma s}&=0.10\rightarrow\lambda_{\sigma s}=\gamma_{\sigma s}+S_{\sigma s}=0.34\,.\end{aligned}\tag{5.22}$$

It is encouraging to see that the total amount of $2p_\pi$ component in the occupied position of the t_{2g} band in V_2O_3 (containing the two t_{2g} electrons) per oxygen site ($\simeq 7\%$) as calculated in Ref. 5 is in reasonable agreement with what we obtain from the calculated value of $\lambda_\pi(=2\times 2\times\frac{1}{12}\lambda_\pi^2=\frac{1}{3}\lambda_\pi^2=9\%)$ (two electrons in the t_{2g} band and two orbitals p_x, p_y of π symmetry). This agreement justifies our estimate for the sum of the last two terms in the right-hand side of (5.20), namely

$$\langle\chi|T+V_{\text{out}}|\phi\rangle-\langle\chi|\phi\rangle\langle\phi|T+V_{\text{out}}+V_{\text{ins}}|\phi\rangle\simeq 0\,.$$

A further quantity, the intra-atomic exchange interaction J must be determined to evaluate the total magnetic moment on the metal ion (5.16) and on the ligand site (5.17). A possible source of information for J comes from the knowledge of the isotopic ligand transferred hyperfine interaction (THI) the strength of which has been measured in Ref. 3. Actually the mere existence of a negative THI is an indication of the existence of process B in Fig. 6. Indeed, since V^{3+} ions have only orbitals of type t_{2g} occupied, the unpaired oxygen $2s$ spin density with polarization opposite to that of the metal ion must come from process B. From the measured value[3] of the fraction of unpaired oxygen $2s$ electrons per moment $2S$ on one-vanadium neighbors we derive the relation

$$(1/2S)f_s=-0.35\times 10^{-3}=-\tfrac{1}{6}(2J/\Delta E)(\gamma_{\sigma s}^2+\gamma_{\sigma s}S_{\sigma s})\,, \tag{5.23}$$

where $2S=1$ because there is only one magnetic electron per V atom. As a matter of fact, according to Ref. 3 the numerical value in (5.23) is, in absolute value, underestimated since positive frequency shifts $\Delta H/H$ due to $2p$-core-polarization hyperfine interaction ($\simeq +0.04\%$) and $2p$-field-induced orbital susceptibility ($\simeq +0.02\%$) have been neglected compared to the measured $\Delta H/H=-0.09\%$. Hence the actual value of f_s in (5.23) might even be a factor of 2 bigger in absolute value. From (5.22) and (5.21) we derive a lower bound to J given by

$$J=7\times 10^{-1}\ \text{eV}\,, \tag{5.24}$$

keeping in mind that J might be underestimated by as much as a factor of 2. [This J should be distinguished from the J introduced in the model Hamiltonian (3.11). This latter is expected to be substantially less than the former since it includes in its definition some polarization of the ligands.] This value of J (5.24) together with the estimated values for γ and S (5.22) allows a numerical evaluation of μ_M in (5.16). Writing the contribution of the various terms separately, we obtain per magnetic electron on the metal ion

$$\mu_M=1-0.28+0.14+0.13+0.04=1.03\,. \tag{5.25}$$

As one can see the covalent reduction due to process A in Fig. 6 ($-\lambda_\pi^2=-0.28$) is slightly outbalanced by the covalency enhancement due to process B. To find the effective magnetic moment one should allow for a further reduction due to itinerancy. We have already anticipated the result of a self-consistent HF calculation with three Wannier states per site. For the set of hopping integrals shown below, we have obtained a magnetic moment per site of approximately 1.0 μ_B in the ground-state configuration. This would seem to imply that the value of J in (5.24) is somewhat underestimated and that as a consequence, the extra (0.2 ± 0.1) μ_B still missing is due to covalency enhancement as suggested in Ref. 3. However, due to the number of approximations used [neglect of the influence of the distortion on the transfer integrals in Hamiltonian (3.11), lack of self-consistency for these latter, use of the HF method to treat interelectronic correlations, especially for electrons inside the vertical pairs, as already pointed out, etc.] it is extremely difficult to say with certainty how much of the observed moment is due to polarization of the a_{1g} electrons and how much to covalency enhancement. For example, a better treatment of the interelectronic correlations would certainly increase the value of the intra-atomic exchange polarization of the a_{1g} electrons compared to that obtained with the unrestricted HF calculations, using the same set of parameters in the model Hamiltonian. Nevertheless, what we should emphasize clearly in our argument above is the importance of the ligand-to-metal-empty-orbital transfer process, if not its necessity to account for the experimental evidence (e.g., a negative ^{17}O nuclear resonance frequency shift). Direct experimental evidence for a negative f_σ due to process B has been given by Freund, Owen, and Hann[23] for Cr^{3+} in MgO where on the basis of process A we would expect $f_\sigma = 0$. Combined neutron scattering and ENDOR measurements of transferred hyperfine interactions have been used to determine the spin transfer coefficients f_s, f_σ, f_π. We feel that in the case of V_2O_3 a similar combination of antiferromagnetic state ^{17}O nuclear resonance studies and spin-density neutron scattering from factor measurements (although difficult) might help decide the relative importance of the two effects discussed above.

Notice in this connection that in the configuration interaction picture the net magnetic moment on a ligand atom is slightly negative [Eqs. (5.17) and (5.25)] due to the nearly compensating effect of process A and B. In a molecular-orbital picture (process A only) the ligand would be polarized parallel to the metal ion, the ratio being $\frac{1}{2}\lambda_\pi^2/(1-\lambda_\pi^2)$. This negative ligand polarization is in keeping with a negative ^{17}O NMR shift observed in the metallic phase of V_2O_3. A similar observation should be possible in the antiferromagnetic insulating phase. We did not invoke an orbital contribution to the observed magnetic moment since, as explained above, the degeneracy of the e_g states is split in the antiferromagnetic ground state because of lack of trigonal symmetry. Hence within a phase factor, the ground state can be chosen to be real with consequent quenching of the orbital moment. This is also borne out by the impossibility which we encountered when attempting to build a self-consistent complex ground state. Every time we tried to start from input averages of the kind

$$\langle c^\dagger_{jm\sigma} c_{jm\sigma}\rangle = \tfrac{1}{2}, \quad m = 1, 2,$$

$$\langle c^\dagger_{jm\sigma} c_{jm'\sigma}\rangle = \pm \tfrac{1}{2} i, \quad m \neq m',$$

indicating occupancy on site j of an orbital of the type $(1/\sqrt{2})(w_1 \pm i w_2)$, the output self-consistent solution was convergent to off-diagonal averages $(m \neq m')$ equal to zero.

Before presenting the results of the HF self-consistent calculations for the general case including both the a_{1g} and e_g states in Hamiltonian (3.11), we would like to point out that the calculated values for the covalency parameters in (5.21) are consistent with what one can derive from measurements of the spin-lattice relaxation rate for ^{17}O in V_2O_3 at $T = 300$ K.[3] Quoting the authors of Ref. 3, "For an oxygen site covalently coupled to four Vanadium neighbors with uncorrelated spin fluctuations and d bands of t_{2g} symmetry, the orbital relaxation rate of ^{17}O can be related to that of ^{51}V by

$$\frac{(1/T_1)_{^{17}\mathrm{O}}}{(1/T_1)_{^{51}\mathrm{V}}} = \frac{4}{3}\left|\frac{\langle r^{-3}\rangle_{2p}}{\langle r^{-3}\rangle_{3d}}\right|^2 \left(\frac{\gamma(^{17}\mathrm{O})}{\gamma(^{51}\mathrm{V})}\right)^2 \left(\frac{f_\pi}{2S}\right)^2 . \text{"} \tag{5.26}$$

This assumes that π covalent transfer is predominant. The factor 4 is the number of Vanadium neighbors, and the factor 3 is a further orbital reduction factor produced by coupling only two of the three t_{2g} orbitals to any one oxygen site.[11] Since all the quantities in (5.26) except $(f_\pi/2S)^2$ are already known or measurable, a value of 0.07 is derived for $|f_\pi/2S|$ by the authors. However, in the light of what we have been discussing up to now, it is apparent that we must modify the relation (5.26) into

$$\frac{(1/T_1)_{^{17}\mathrm{O}}}{(1/T_1)_{^{51}\mathrm{V}}} = 4\left|\frac{\langle r^{-3}\rangle_{2p}}{\langle r^{-3}\rangle_{3d}}\right|^2 \left(\frac{\gamma(^{17}\mathrm{O})}{\gamma(^{51}\mathrm{V})}\right)^2 \frac{1}{2S} \times [(f_\pi^A)^2 + (f_\pi^B)^2 + (f_\sigma^B)^2], \tag{5.27}$$

where we have eliminated the factor 3 in the denominator since all the $3d$ orbitals are now coupled to every oxygen site and f_π^A indicates the fraction of ligand unpaired spin coming from process A in Fig. 6 as opposed to f_π^B which comes from process B. From the definition of the quantities f we easily calculate ($2S=1$)

$$\begin{aligned} f_\pi^A &= \tfrac{1}{12}\lambda_\pi^2 = 2.5\times 10^{-2}, \\ f_\pi^B &= \tfrac{1}{12}(2J/\Delta E)(\gamma_\pi^2+\gamma_\pi S_\pi) = 1.1\times 10^{-2}, \\ f_\sigma^B &= \tfrac{1}{6}(2J/\Delta E)(\gamma_\sigma^2+\gamma_\sigma S_\sigma) = 1.1\times 10^{-2}, \end{aligned} \tag{5.28}$$

and find

$$(f_\pi^A)^2+(f_\pi^B)^2+(f_\sigma^B)^2 = 8.7\times 10^{-4} \tag{5.29}$$

in reasonable agreement with that derived from (5.27) i.e., $\frac{1}{3}(7\times 10^{-2})^2 = 13\times 10^{-4}$ considering the uncertainty in the covalency reduction of $\langle r_{3d}^{-3}\rangle$. The authors in Ref. 3 reduce this quantity from 3.36 a.u. to 2.8 a.u. because of covalency. However, if we take into account process B as well as process A of Fig. 6 and calculate the amount of charge transferred back to the V^{3+} ion we see that the V atom is nearly neutral, only 0.5 electrons are missing. Hence $\langle r_{3d}^{-3}\rangle$ should not be reduced that much by covalency which would bring the measured value for the last quantity in (5.27) nearer to our estimated value in (5.29).

VI. RESULTS OF THE HF CALCULATION IN THE INSULATING PHASE FOR THE GENERAL CASE

We are now in a position to present the self-consistent HF calculations for the general case. As already mentioned, due to the complexity of the problem, it is imperative that we keep the number of parameters down. As far as the overlap integrals are concerned, on the basis of (2.16) and (2.17) by taking $\lambda_\pi^2 \simeq 0.3$ and $\Delta E \simeq 4$ eV we obtain

$$\begin{aligned} &\mu = 0.24/1.2 = 0.2\ , && \nu = -0.05/1.2 = -0.042\ , \\ &-\alpha = -0.16/1.2 = -0.13\ , && \pi = 0.01/1.2 = 0.008\ , \\ &\beta = -0.05/1.2 = -0.04, && \delta = 0.12/1.2 = 0.1\ , \\ &\rho = -0.86/1.2 = -0.72\ , && \epsilon = -0.17/1.2 = 0.14\ , \\ &\sigma = 0.06/1.2 = 0.05\ , && \lambda = 0.04/1.2 = 0.03\ , \\ &-\tau = -0.28/1.2 = -0.23\ , && \omega = -0.16/1.2 = -0.13\ . \end{aligned} \tag{6.1}$$

Actually, the values given in (6.1) should be taken as orientative values. The transfer integrals given in (2.17) are calculated from Ref. 5, keeping the potential V_{out} outside the muffin-tin spheres equal to zero (V_{out} is kept as a parameter in Ref. 5) to account for the contribution of the kinetic-energy operator neglected in the calculation of the $(3d, 3d)$ matrix elements and is determined such as to obtain best fit of calculated density of states with optical measurements. Account must be taken for the fact that our approach is a kind of perturbation-theory approximation to the more complete calculations of Ref. 5; moreover, the effect of the trigonal distortion of the surrounding octahedra of a metal ion has been neglected as well as the energy dependence of λ_π (the e_g band is approximately 3–4 eV wide). Thus we have (somewhat) changed the values in (6.1) to obtain a calculated density of states better fitting than that given in Ref. 5, at least as far as the distances between the peaks are concerned, which is what matters most in a comparison with optical experiments.

The resulting bare-band density of states is shown in Fig. 7 together with the values of the transfer integrals which have been used for the self-consistent HF calculations. The most distinct and important feature of this set is that the transfer integral ρ along the vertical pairs of a_{1g} state is, in absolute value, twice the next biggest overlap integral. Within a reasonable variation of the parameters in (2.16) it is a well established fact that $|\rho|$ must be substantially bigger than all the other transfer integrals, mainly because the interference between bare $(3d, 3d)$ transfer and covalent transfer is constructive, contrary to what happens for all the other quantities in (2.16), except for τ which in any case is less favored both by the orientation of the $3d$

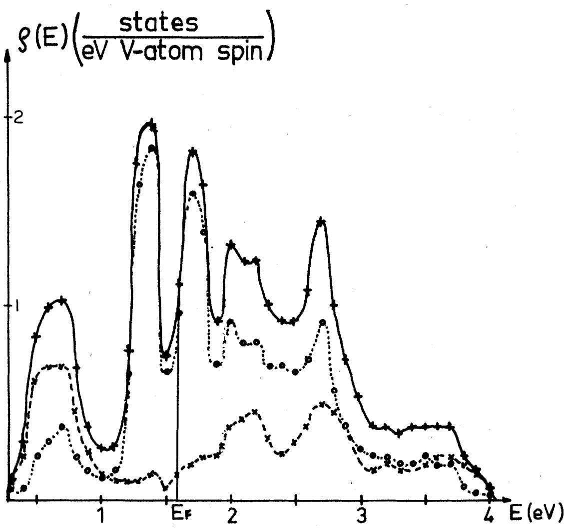

FIG. 7. Bare band density of the states curve (full curve) together with the partial density of the states curves of e_g character (dotted curve) and a_{1g} character (dashed curve). The values of the transfer integrals used in this calculation are (in eV) $\mu=0.40$, $\alpha=0.28$, $\beta=0.10$, $\rho=-0.75$, $\sigma=0.06$, $\tau=0.30$, $\nu=-0.04$, $\pi=0.012$, $\delta=0.011$, $\epsilon=-0.125$, $\lambda=0.025$, $\omega=-0.125$.

orbitals and by smaller covalency contribution. This is an important fact to note because our conclusions in the following are not affected by reasonable variations of the other overlap integrals, but do strongly depend on whether or not $|\rho|$ is substantially bigger (a factor 1.5 or more) than the other quantities.

The fact that ρ is so big suggests the idea of diamagnetic pairs along the vertical direction for a_{1g} electrons. However, since it will turn out that $2|\rho| \simeq U$, we shall be faced with the problem of best describing the correlation inside the vertical pairs. As discussed at length in Sec. I of this paper, we know that the best HF approximation for a diamagnetic pair is a molecular-orbital wave function (state a) in (1.18) for $2|\rho| > U$ whereas a spin-density-wave state, although fictitious, is most appropriate for $2|\rho| < U$. Hence in all those cases for which $2|\rho| < U$, we should use an antiferromagnetic-spin (AS) structure to best describe the correlations in the a_{1g} band. However, this fictitious structure tends to polarize by intra-atomic exchange the electron in the e_g band, making the AO(1)-AS(e_g)AS(a_{1g}) state competitive in energy with the AO(1)-RS(e_g)PS(a_{1g}) state, the one that we consider to realistically represent the features of the true ground state in the antiferromagnetic insulating phase of V_2O_3. In support of this conjecture stands the fact that if the ratio $U/2|\rho|$ is decreased the AO(1)-AS(e_g)AS(a_{1g}) state increases its energy compared to the other.

Having thus fixed the values of the overlap integrals, the only parameters left are U and J/U, since we can eliminate U' on the basis of the relation (3.13). As a matter of fact from the Stoner enhancement factor derived from susceptibility measurements as will be discussed at length in III, we derive a further relation $U+J \simeq 2$ eV. Hence we choose to move the parameters U and J/U so that they approximately satisfy this relation and we take reasonably $0.1 \lesssim J/U \lesssim 0.2$.

The results of the self-consistent HF calculations in the general case with the a_{1g} band included can then be summarized as follows: For $J/U < 0.15$, the AO(1)-RS structure for e_g electrons and a diamagnetic a_{1g} band (PS) is found to be the most stable (lowest ground-state energy) configurations among various possible self-consistent structures which we tried. For U big enough, a gap opens in the density of states (Fig. 9) which is of the order of 0.2 eV for $U+J \simeq 2$ eV and $J/U \simeq 0.1$. The amount of polarization of the a_{1g} band by the e_g band depends on the ratio J/U and the position of the a_{1g} atomic level compared to the e_g level. By slightly varying these parameters (together with $|\rho|$) one can change the amount of polarization as much as 100% from 0.1 to 0.2 electrons per site.

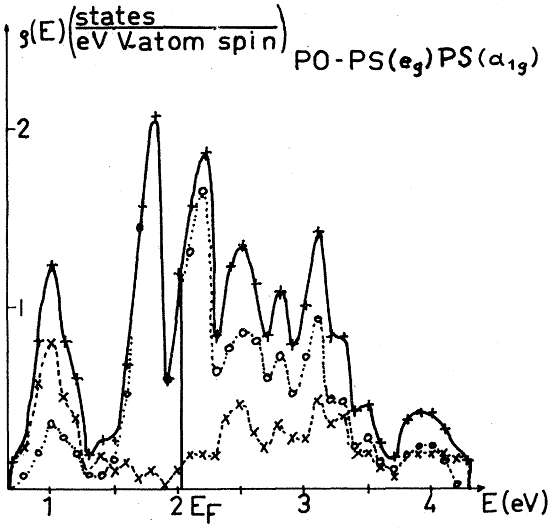

FIG. 8. Total density of the states curve for the configuration PO-PS(e_g)PS(a_{1g}) of Table V for the case $U = 1.80$, $U' = 1.44$, $J = 0.18$. Also shown are the partial density of the states curves for e_g (curve with circles) and a_{1g} (curve with crosses) electrons.

By increasing the ratio $J/U (\simeq 0.2)$, the number of possible self-consistent HF configurations is reduced in the sense that several input configurations merge into a single one at self-consistency. Moreover, it appears that the most stable self-consistent solution is the one in which the e_g band contains 1.5 electrons per site, is ordered in the RS structure and obviously not orbitally ordered, whereas the a_{1g} band is half full with 0.5 electrons per site and polarized in the same spin

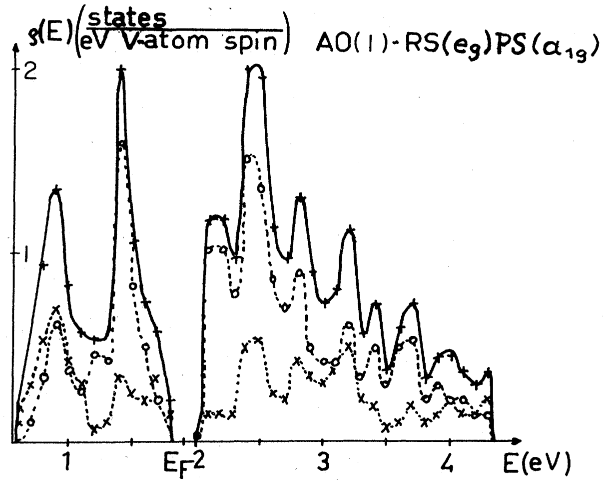

FIG. 9. Same as Fig. 8 for the configuration AO(1)–RS (e_g)PS(a_{1g}).

structure. The moment is 1.7 μ_B per site and should be reduced by the covalency factor $(1-\lambda_\pi^2/2)$ leading to a net result of 1.45 μ_B per site, in marked disagreement with the experimental findings, not considering, as already mentioned, the influence of the back-bonding processes described in Sec. V, which would tend to increase it. Moreover, this state is metallic, since now we must put 0.5 electrons in the e_g band above the point where it would be easy to open a correlation gap (Fig. 10). It would nevertheless still be possible to open a gap even in this second case by invoking the distortion taking place in the antiferromagnetic insulator phase of V_2O_3. In fact up to now, we have considered the transfer integrals as transforming according to the trigonal symmetry. If we take into account the fact that the crystal symmetry, not only the magnetic symmetry, is lower, we are forced to introduce new transfer integrals (proportional to the distortion for small displacements of the atoms). Using them as parameters and modifying the preexisting transfer integrals according to the distortion, we are able to open a gap. This is the picture which we presented previously in Ref. 20. However, it should be realized that from this point of view, the negative value of f_s in (5.23) would remain unexplained without invoking process B in Fig. 6 and the value of the negative moment per site would turn out to be too big, whether or not process B is considered. Moreover the gap found is extremely small (0.05 eV) and it is difficult to increase it by relying only on the distortion of the lattice. For these reasons we are inclined to believe the picture where the J/U ratio is small enough as to make the AO(1)-RS(e_g)RS(a_{1g}) state the true ground state, with one magnetic electron per site in a e_g band partly polarizing the a_{1g} band electrons and the magnetic moment per site being enhanced by covalency. In this view the distortion is purely magnetostrictive in origin having little influence on the opening of the gap which is primarily caused by electron correlation.

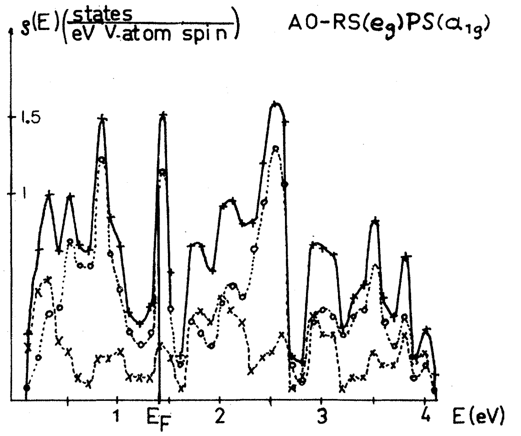

FIG. 10. Same as Fig. 9, for $U=2.0$, $U'=1.2$, $J=0.4$.

Table V gives the ground-state energies in eV per mole of V_2O_3 for various configurations and different values for U and J/U. Included also is the state PO-PS(e_g)PS(a_{1g}) which for the case of three states per site is strictly speaking no more equivalent to a bare band-structure calculation although the two densities of states are quite similar (Fig. 8). The reason is that the additional a_{1g} state is not equivalent to the other two e_g so that optimum occupancy of the three types of bands must be sought according to the reciprocal shift of the two atomic levels and the ratio J/U. In the spirit of the HF approximation, this state should represent the metallic phase of V_2O_3. We shall discuss at length, in III, the properties of the metallic phase. For easier understanding of the notation of the configuration quoted in Table V, Tables VI–XI give the occupation numbers for the

TABLE V. Illustration of the ground-state energy and gap in the density of states for various ground-state configurations. Values of the hopping integrals are those given in expression (6.2). Dots indicate the impossibility of opening a gap while the value 0.0 in the column for $\Delta\epsilon_g$ indicates that a gap can be opened by a small increase of U or that the gap is less than 0.05 eV.

U	2.0		2.0		1.80		1.50	
U'	1.6		1.2		1.44		1.30	
J	0.2		0.4		0.18		0.15	
eV/molecule V_2O_3	E_G	$\Delta\epsilon_g$	E_G	$\Delta\epsilon_g$	E_G	$\Delta\epsilon_g$	E_G	$\Delta\epsilon_g$
AO−RS(e_g)PS(a_{1g})	1.408	0.3	0.0341	···	0.960	0.20	0.256	0.0
AO−AS(e_g)AS(a_{1g})	1.407	0.3	0.160	0.0	0.981	0.15	0.297	···
AO−RS(e_g)RS(a_{1g})	1.461	···	0.0341	···	0.960	0.20	0.262	···
2RS(e_g)	1.477	···	0.0341	···	0.975	0.0	0.262	···
AO−RS(e_g)AS(a_{1g})	1.420	0.2	0.072	···	0.967	0.15	0.259	0.0
PO−PS(e_g)PS(a_{1g})	1.650	···	0.319	···	1.115	···	0.316	···

TABLE VI (a). Self-consistently determined unrestricted HF occupation numbers and off-diagonal elements $\langle c^{\dagger}_{\alpha m\uparrow} c_{\alpha n\uparrow}\rangle$ ($m,n=1,2,3$) for spin-up electrons appear underneath the corresponding input parameters which have been used to characterize the AO(1)–RS(e_g) PS(a_{1g}) structure; (b) Self-consistently determined unrestricted HF occupation numbers and off-diagonal elements $\langle c^{\dagger}_{\alpha m\downarrow} c_{\alpha n\downarrow}\rangle$ ($m,n=1,2,3$) for spin-down electrons appears underneath the corresponding input parameters which have been used to characterize the AO(1)–RS(e_g) PS(a_{1g}) structure; (c) Spin and charge distribution for the eight V atoms in the rhombohedral unit cell for the AO(1)–RS(e_g) PS(a_{1g}) structure.

(a)

m *n* \ Site	1	2	3	4	5	6	7	8
1 1	1.0 0.792	0.0 0.302	0.0 0.046	0.0 0.302	1.0 0.792	0.0 0.063	0.0 0.063	0.0 0.046
2 1	0.0 0.039	0.0 0.023	0.0 0.001	0.0 −0.023	0.0 −0.039	0.0 0.006	0.0 −0.006	0.0 −0.001
3 1	0.0 0.004	0.0 0.001	0.0 −0.003	0.0 −0.001	0.0 −0.004	0.0 0.006	0.0 −0.006	0.0 0.003
1 2	0.0 0.039	0.0 0.023	0.0 0.001	0.0 −0.023	0.0 −0.039	0.0 0.006	0.0 −0.006	0.0 −0.001
2 2	0.0 0.220	1.0 0.807	0.0 0.059	1.0 0.807	0.0 0.220	0.0 0.104	0.0 0.104	0.0 0.059
3 2	0.0 −0.008	0.0 0.023	0.0 −0.029	0.0 0.023	0.0 −0.008	0.0 0.062	0.0 0.062	0.0 −0.029
1 3	0.0 0.004	0.0 0.001	0.0 −0.003	0.0 −0.001	0.0 −0.004	0.0 0.006	0.0 −0.006	0.0 0.003
2 3	0.0 −0.008	0.0 0.023	0.0 −0.029	0.0 0.023	0.0 −0.008	0.0 0.062	0.0 0.062	0.0 −0.029
3 3	0.5 0.336	0.5 0.513	0.5 0.288	0.5 0.513	0.5 0.336	0.5 0.467	0.5 0.467	0.5 0.288

(b)

m *n* \ Site	1	2	3	4	5	6	7	8
1 1	0.0 0.063	0.0 0.046	0.0 0.302	0.0 0.046	0.0 0.063	1.0 0.792	1.0 0.792	0.0 0.302
2 1	0.0 −0.006	0.0 0.001	0.0 0.023	0.0 −0.001	0.0 0.006	0.0 −0.039	0.0 0.039	0.0 −0.023
3 1	0.0 −0.006	0.0 −0.003	0.0 0.001	0.0 0.003	0.0 0.006	0.0 −0.004	0.0 0.004	0.0 −0.001
1 2	0.0 −0.006	0.0 0.001	0.0 0.023	0.0 −0.001	0.0 0.006	0.0 −0.039	0.0 0.039	0.0 −0.023
2 2	0.0 0.104	0.0 0.059	1.0 0.807	0.0 0.059	0.0 0.104	0.0 0.220	0.0 0.220	1.0 0.807
3 2	0.0 0.062	0.0 −0.029	0.0 0.023	0.0 −0.029	0.0 0.062	0.0 −0.008	0.0 −0.008	0.0 0.023
1 3	0.0 −0.006	0.0 −0.003	0.0 0.001	0.0 0.003	0.0 0.006	0.0 −0.004	0.0 0.004	0.0 −0.001
2 3	0.0 0.062	0.0 −0.029	0.0 0.023	0.0 −0.029	0.0 0.062	0.0 −0.008	0.0 −0.008	0.0 0.023
3 3	0.5 0.467	0.5 0.289	0.5 0.513	0.5 0.289	0.5 0.467	0.5 0.337	0.5 0.337	0.5 0.513

(c)

Spin	0.715	1.228	−1.228	1.228	0.715	−0.715	−0.715	−1.228
Charge	1.983	2.017	2.017	2.017	1.983	1.983	1.983	2.017

TABLE VII(a). Same as in Table VI (a) for the AO(1)−S(e_g)AS(a_{1g}) structure; (b) Same as in Table VI (b). for the AO(1)−AS(e_g)AS(a_{1g}) structure; (c) Same as in Table VI (c) for the AO(1)−AS(e_g)AS(a_{1g}) structure.

(a)

m n \ Site	1	2	3	4	5	6	7	8
1 1	0.0	0.0	0.0	0.0	0.0	0.0	0.0	0.0
	0.061	0.063	0.063	0.063	0.061	0.061	0.061	0.063
2 1	0.0	0.0	0.0	0.0	0.0	0.0	0.0	0.0
	−0.006	−0.006	−0.006	0.006	0.006	0.006	−0.006	0.006
3 1	0.0	0.0	0.0	0.0	0.0	0.0	0.0	0.0
	−0.002	−0.006	−0.006	0.006	0.002	0.002	−0.002	0.006
1 2	0.0	0.0	0.0	0.0	0.0	0.0	0.0	0.0
	−0.006	−0.006	−0.006	0.006	0.006	0.006	−0.006	0.006
2 2	0.0	1.0	1.0	1.0	0.0	0.0	0.0	1.0
	0.164	0.858	0.858	0.858	0.164	0.164	0.164	0.858
3 2	0.0	0.0	0.0	0.0	0.0	0.0	0.0	0.0
	0.004	0.033	0.033	0.033	0.004	0.004	0.004	0.033
1 3	0.0	0.0	0.0	0.0	0.0	0.0	0.0	0.0
	−0.002	−0.006	−0.006	0.006	0.002	0.002	−0.002	0.006
2 3	0.0	0.0	0.0	0.0	0.0	0.0	0.0	0.0
	0.004	0.033	0.033	0.033	0.004	0.004	0.004	0.033
3 3	0.0	1.0	1.0	1.0	0.0	0.0	0.0	1.0
	0.239	0.615	0.615	0.615	0.239	0.239	0.239	0.615

(b)

m n \ Site	1	2	3	4	5	6	7	8
1 1	1.0	0.0	0.0	0.0	1.0	1.0	1.0	0.0
	0.861	0.174	0.174	0.174	0.861	0.861	0.861	0.174
2 1	0.0	0.0	0.0	0.0	0.0	0.0	0.0	0.0
	0.020	0.001	0.001	−0.001	−0.020	−0.020	0.020	−0.001
3 1	0.0	0.0	0.0	0.0	0.0	0.0	0.0	0.0
	−0.005	0.002	0.002	−0.002	0.005	0.005	−0.005	−0.002
1 2	0.0	0.0	0.0	0.0	0.0	0.0	0.0	0.0
	0.020	0.001	0.001	−0.001	−0.020	−0.020	0.020	−0.001
2 2	0.0	0.0	0.0	0.0	0.0	0.0	0.0	0.0
	0.072	0.057	0.057	0.057	0.072	0.072	0.072	0.057
3 2	0.0	0.0	0.0	0.0	0.0	0.0	0.0	0.0
	0.050	−0.017	−0.017	−0.017	0.050	0.050	0.050	−0.017
1 3	0.0	0.0	0.0	0.0	0.0	0.0	0.0	0.0
	−0.005	0.002	0.002	−0.002	0.005	0.005	−0.005	−0.002
2 3	0.0	0.0	0.0	0.0	0.0	0.0	0.0	0.0
	0.050	−0.017	−0.017	−0.017	0.050	0.050	0.050	−0.017
3 3	1.0	0.0	0.0	0.0	1.0	1.0	1.0	0.0
	0.602	0.235	0.235	0.235	0.602	0.602	0.602	0.235

(c)

Spin	−1.070	1.070	1.070	1.070	−1.070	−1.070	−1.070	1.070
Charge	1.998	2.002	2.002	2.002	1.998	1.998	1.998	2.002

TABLE VIII. (a). Same as in Table VI (a) for the AO(1)–RS(e_g)RS(a_{1g}) structure; (b) Same as in Table VI (b) for the AO(1)–RS(e_g)RS(a_{1g}) structure; (c) Same as in Table VI (c) For the AO(1)—RS(e_g)RS(a_{1g}) structure.

(a)

m n \ Site	1	2	3	4	5	6	7	8
1 1	1.0	0.0	0.0	0.0	1.0	0.0	0.0	0.0
	0.793	0.301	0.047	0.301	0.793	0.063	0.063	0.047
2 1	0.0	0.0	0.0	0.0	0.0	0.0	0.0	0.0
	0.037	0.021	0.001	−0.021	−0.037	0.006	−0.006	−0.001
3 1	0.0	0.0	0.0	0.0	0.0	0.0	0.0	0.0
	0.004	0.001	−0.002	−0.001	−0.004	0.006	−0.006	0.002
1 2	0.0	0.0	0.0	0.0	0.0	0.0	0.0	0.0
	0.037	0.021	0.001	−0.021	−0.037	0.006	−0.006	−0.001
2 2	0.0	1.0	0.0	1.0	0.0	0.0	0.0	0.0
	0.223	0.806	0.060	0.806	0.223	0.104	0.104	0.060
3 2	0.0	0.0	0.0	0.0	0.0	0.0	0.0	0.0
	−0.006	0.024	−0.030	0.024	−0.007	0.061	0.061	−0.030
1 3	0.0	0.0	0.0	0.0	0.0	0.0	0.0	0.0
	0.004	0.001	−0.002	−0.001	−0.004	0.006	−0.006	0.002
2 3	0.0	0.0	0.0	0.0	0.0	0.0	0.0	0.0
	−0.007	0.024	−0.030	0.024	−0.007	0.061	0.061	−0.030
3 3	1.0	1.0	0.0	1.0	1.0	0.0	0.0	0.0
	0.341	0.508	0.291	0.508	0.341	0.464	0.464	0.291

(b)

m n \ Site	1	2	3	4	5	6	7	8
1 1	0.0	0.0	0.0	0.0	0.0	1.0	1.0	0.0
	0.063	0.047	0.301	0.047	0.063	0.793	0.793	0.301
2 1	0.0	0.0	0.0	0.0	0.0	0.0	0.0	0.0
	−0.006	0.001	0.021	−0.001	0.006	−0.037	0.037	−0.021
3 1	0.0	0.0	0.0	0.0	0.0	0.0	0.0	0.0
	−0.006	−0.002	0.001	0.002	0.006	−0.004	0.004	−0.001
1 2	0.0	0.0	0.0	0.0	0.0	0.0	0.0	0.0
	−0.006	0.001	0.021	−0.001	0.006	−0.037	0.032	−0.021
2 2	0.0	0.0	1.0	0.0	0.0	0.0	0.0	1.0
	0.104	0.059	0.805	0.059	0.104	0.223	0.223	0.805
3 2	0.0	0.0	0.0	0.0	0.0	0.0	0.0	0.0
	0.061	−0.030	0.024	−0.030	0.061	−0.007	−0.007	0.024
1 3	0.0	0.0	0.0	0.0	0.0	0.0	0.0	0.0
	−0.006	−0.002	0.001	0.002	0.006	−0.004	0.004	−0.001
2 3	0.0	0.0	0.0	0.0	0.0	0.0	0.0	0.0
	0.061	−0.030	0.024	−0.030	0.061	−0.007	−0.001	0.024
3 3	0.0	0.0	1.0	0.0	0.0	1.0	1.0	1.0
	0.464	0.291	0.508	0.291	0.464	0.341	0.341	0.508

(c)

Spin	0.725	1.217	−1.217	1.217	0.725	−0.725	−0.725	−1.217
Charge	1.988	2.012	2.012	2.012	1.987	1.987	1.987	2.012

TABLE IX (a). Same as in Table VI (a) for the 2 RS(e_g) structure; (b) Same as in Table VI (b) for the 2 RS (e_g) structure; (c) Same as in Table VI (c) for the 2 RS (e_g) structure.

(a)

m n \ Site	1	2	3	4	5	6	7	8
1 1	1.0	1.0	0.0	1.0	1.0	0.0	0.0	0.0
	0.543	0.543	0.068	0.543	0.543	0.069	0.068	0.069
2 1	0.0	0.0	0.0	0.0	0.0	0.0	0.0	0.0
	0.179	0.179	−0.007	−0.179	−0.179	0.007	−0.007	0.007
3 1	0.0	0.0	0.0	0.0	0.0	0.0	0.0	0.0
	0.010	0.010	−0.017	−0.010	−0.010	0.017	−0.017	0.017
1 2	0.0	0.0	0.0	0.0	0.0	0.0	0.0	0.0
	0.179	0.179	−0.007	−0.179	−0.179	0.007	−0.007	0.007
2 2	1.0	1.0	0.0	1.0	1.0	0.0	0.0	0.0
	0.543	0.543	0.068	0.543	0.543	0.068	0.068	0.068
3 2	0.0	0.0	0.0	0.0	0.0	0.0	0.0	0.0
	0.047	0.047	−0.012	0.047	0.047	−0.012	−0.012	−0.012
1 3	0.0	0.0	0.0	0.0	0.0	0.0	0.0	0.0
	0.010	0.010	−0.017	−0.010	−0.010	0.017	−0.017	0.017
2 3	0.0	0.0	0.0	0.0	0.0	0.0	0.0	0.0
	0.047	0.047	−0.012	0.047	0.047	−0.012	−0.012	−0.012
3 3	0.0	0.0	0.0	0.0	0.0	0.0	0.0	0.0
	0.416	0.416	0.360	0.416	0.416	0.360	0.360	0.360

(b)

m n \ Site	1	2	3	4	5	6	7	8
1 1	0.0	0.0	1.0	0.0	0.0	1.0	1.0	1.0
	0.068	0.068	0.543	0.068	0.068	0.543	0.543	0.543
2 1	0.0	0.0	0.0	0.0	0.0	0.0	0.0	0.0
	0.007	−0.007	0.179	0.007	0.007	−0.179	0.179	−0.179
3 1	0.0	0.0	0.0	0.0	0.0	0.0	0.0	0.0
	0.017	−0.017	0.010	0.017	0.017	−0.010	0.010	−0.010
1 2	0.0	0.0	0.0	0.0	0.0	0.0	0.0	0.0
	0.007	−0.007	0.179	0.007	0.007	−0.179	0.179	−0.179
2 2	0.0	0.0	1.0	0.0	0.0	1.0	1.0	1.0
	0.068	0.068	0.543	0.068	0.068	0.543	0.543	0.543
3 2	0.0	0.0	0.0	0.0	0.0	0.0	0.0	0.0
	0.012	−0.012	0.047	−0.012	−0.012	0.047	0.047	0.047
1 3	0.0	0.0	0.0	0.0	0.0	0.0	0.0	0.0
	0.017	−0.017	0.010	0.017	0.017	−0.010	0.010	−0.010
2 3	0.0	0.0	0.0	0.0	0.0	0.0	0.0	0.0
	0.012	−0.012	0.047	−0.012	−0.012	0.047	0.047	0.047
3 3	0.0	0.0	0.0	0.0	0.0	0.0	0.0	0.0
	0.360	0.360	0.416	0.360	0.360	0.416	0.416	0.416

(c)

Spin	1.006	1.006	−1.006	1.006	1.006	−1.006	−1.006	−1.006
Charge	2.000	2.000	2.000	2.000	2.000	2.000	2.000	2.000

TABLE X (a). Same as in Table VI (a) for the AO(1)–RS(e_g)AS(a_{1g}) structure; (b) Same as in Table VI (b) for the AO(1)—RS (e_g)AS(a_{1g}) structure; (c) Same as in Table VI (c) for the AO(1)—RS(e_g) AS (a_{1g}) structure.

(a)

m n \ Site	1	2	3	4	5	6	7	8
1 1	1.0	0.0	0.0	0.0	1.0	0.0	0.0	0.0
	0.782	0.296	0.052	0.296	0.782	0.059	0.059	0.052
2 1	0.0	0.0	0.0	0.0	0.0	0.0	0.0	0.0
	0.021	0.009	0.001	−0.009	−0.021	0.004	−0.004	−0.001
3 1	0.0	0.0	0.0	0.0	0.0	0.0	0.0	0.0
	0.007	−0.002	−0.005	0.002	−0.006	0.003	−0.003	0.005
1 2	0.0	0.0	0.0	0.0	0.0	0.0	0.0	0.0
	0.021	0.009	0.001	−0.009	−0.021	0.004	−0.004	−0.001
2 2	0.0	1.0	0.0	1.0	0.0	0.0	0.0	0.0
	0.221	0.816	0.066	0.816	0.221	0.098	0.098	0.066
3 2	0.0	0.0	0.0	0.0	0.0	0.0	0.0	0.0
	0.000	0.027	−0.054	0.027	0.000	0.029	0.029	−0.054
1 3	0.0	0.0	0.0	0.0	0.0	0.0	0.0	0.0
	0.007	−0.002	−0.005	0.002	−0.006	0.003	−0.003	0.005
2 3	0.0	0.0	0.0	0.0	0.0	0.0	0.0	0.0
	0.000	0.027	−0.054	0.027	0.000	0.029	0.029	−0.054
3 3	0.0	1.0	1.0	1.0	0.0	0.0	0.0	1.0
	0.306	0.545	0.432	0.545	0.306	0.326	0.326	0.432

(b)

m n \ Site	1	2	3	4	5	6	7	8
1 1	0.0	0.0	0.0	0.0	0.0	1.0	1.0	0.0
	0.062	0.052	0.273	0.052	0.062	0.815	0.815	0.273
2 1	0.0	0.0	0.0	0.0	0.0	0.0	0.0	0.0
	−0.004	0.001	0.009	−0.001	0.004	−0.021	0.021	−0.009
3 1	0.0	0.0	0.0	0.0	0.0	0.0	0.0	0.0
	−0.006	−0.001	0.002	0.001	0.006	−0.000	0.000	−0.002
1 2	0.0	0.0	0.0	0.0	0.0	0.0	0.0	0.0
	−0.004	0.001	0.009	−0.001	0.004	−0.021	0.021	−0.009
2 2	0.0	0.0	1.0	0.0	0.0	0.0	0.0	1.0
	0.102	0.056	0.794	0.056	0.102	0.230	0.230	0.794
3 2	0.0	0.0	0.0	0.0	0.0	0.0	0.0	0.0
	0.070	−0.024	0.037	−0.024	0.070	0.016	0.016	0.037
1 3	0.0	0.0	0.0	0.0	0.0	0.0	0.0	0.0
	−0.006	−0.001	0.002	0.001	0.006	0.000	0.000	−0.002
2 3	0.0	0.0	0.0	0.0	0.0	0.0	0.0	0.0
	0.070	−0.024	0.037	−0.024	0.070	0.016	0.016	0.037
3 3	1.0	0.0	0.0	0.0	1.0	1.0	1.0	0.0
	0.516	0.254	0.384	0.254	0.516	0.462	0.462	0.384

(c)

Spin	0.628	1.295	−0.901	1.295	0.628	−1.023	−1.023	−0.901
Charge	1.990	2.020	2.000	2.020	1.990	1.990	1.990	2.000

TABLE XI (a). Same as in Table VI (a) for the PO-PS (e_g)PS(a_{1g}) structure; (b) Same as in Table VI (b) for the PO-PS(e_g)PS(a_{1g}) structure; (c) Same as in Table VI (c) for the PO-PS (e_g)PS(a_{1g}) structure.

(a)

Site m n	1	2	3	4	5	6	7	8
1 1	0.25	0.25	0.25	0.25	0.25	0.25	0.25	0.25
	0.318	0.318	0.318	0.318	0.318	0.318	0.318	0.318
2 1	0.0	0.0	0.0	0.0	0.0	0.0	0.0	0.0
	0.000	0.000	0.000	0.000	0.000	0.000	0.000	0.000
3 1	0.0	0.0	0.0	0.0	0.0	0.0	0.0	0.0
	0.002	0.002	0.002	−0.002	−0.002	−0.002	0.002	−0.002
1 2	0.0	0.0	0.0	0.0	0.0	0.0	0.0	0.0
	0.000	0.000	0.000	0.000	0.000	0.000	0.000	0.000
2 2	0.25	0.25	0.25	0.25	0.25	0.25	0.25	0.25
	0.308	0.308	0.308	0.308	0.308	0.308	0.308	0.308
3 2	0.0	0.0	0.0	0.0	0.0	0.0	0.0	0.0
	0.001	0.001	0.001	0.001	0.001	0.001	0.001	0.001
1 3	0.0	0.0	0.0	0.0	0.0	0.0	0.0	0.0
	0.002	0.002	0.002	−0.002	−0.002	−0.002	0.002	−0.002
2 3	0.0	0.0	0.0	0.0	0.0	0.0	0.0	0.0
	0.001	0.001	0.001	0.001	0.001	0.001	0.001	0.001
3 3	0.5	0.5	0.5	0.5	0.5	0.5	0.5	0.5
	0.375	0.375	0.375	0.375	0.375	0.375	0.375	0.375

(b)

Site m n	1	2	3	4	5	6	7	8
1 1	0.25	0.25	0.25	0.25	0.25	0.25	0.25	0.25
	0.318	0.318	0.318	0.318	0.318	0.318	0.318	0.318
2 1	0.0	0.0	0.0	0.0	0.0	0.0	0.0	0.0
	0.000	0.000	0.000	0.000	0.000	0.000	0.000	0.000
3 1	0.0	0.0	0.0	0.0	0.0	0.0	0.0	0.0
	0.002	0.002	0.002	−0.002	−0.002	−0.002	0.002	-0.002
1 2	0.0	0.0	0.0	0.0	0.0	0.0	0.0	0.0
	0.000	0.000	0.000	0.000	0.000	0.000	0.000	0.000
2 2	0.25	0.25	0.25	0.25	0.25	0.25	0.25	0.25
	0.308	0.308	0.308	0.308	0.308	0.308	0.308	0.308
3 2	0.0	0.0	0.0	0.0	0.0	0.0	0.0	0.0
	0.001	0.001	0.001	0.001	0.001	0.001	0.001	0.001
1 3	0.0	0.0	0.0	0.0	0.0	0.0	0.0	0.0
	0.002	0.002	0.002	−0.002	−0.002	−0.002	0.002	−0.002
2 3	0.0	0.0	0.0	0.0	0.0	0.0	0.0	0.0
	0.001	0.001	0.001	0.001	0.001	0.001	0.001	0.001
3 3	0.5	0.5	0.5	0.5	0.5	0.5	0.5	0.5
	0.375	0.375	0.375	0.375	0.375	0.375	0.375	0.375

(c)

Spin	0.000	0.000	0.000	0.000	0.000	0.000	0.000	0.000
Charge	2.000	2.000	2.000	2.000	2.000	2.000	2.000	2.000

electrons relative to the eight sites in the monoclinic unit cell (Fig. 3 of I) for the case $U = 1.80$, $U' = 1.44$, and $J = 0.18$. They are self-explanatory. There is only one more comment in order. Although we start with a paramagnetic type of occupation number for a_{1g} electrons, as for example in the AO(1)-RS(e_g)PS(a_{1g}) state, the self-consistent solution shows an antiferromagnetic type of correlation between a_{1g} electrons in the vertical pairs. As discussed at length in Sec. I, this type of correlation is an artifact of the unrestricted HF method. It reflects only the fact that at self-consistency $2\rho_{\text{eff}}/U_{\text{eff}} < 1$ for a_{1g} electrons, so that intramolecular correlations are better described by a spin-density-wave solution. The antiferromagnetic arrangement within vertical pairs leads to the apparently "crazy" distribution of total spin occupation numbers per site in Table VI.

The way to interpret the results should however be clear from the preceding discussion in this paper. We have to consider the a_{1g} band paramagnetic (e.g. in Table VI there are $\simeq 0.33 a_{1g}$ electron in the up-spin state on site 1 and $\simeq 0.47$ in the down-spin states), the missing electrons necessary to make up one electron per site having been promoted to the e_g band by intra-atomic exchange correlation.

VII. CONCLUSION

It is perhaps instructive to conclude this second paper with a comparison of the low-temperature phases of the corundum structure compounds Ti_2O_3, V_2O_3, and Cr_2O_3. Indeed the formulas for the relevant effective transfer integrals of Eq. (2.16) apply as well to $3dt_{2g}$ electrons in any corundum structure compounds, provided $\lambda_\pi^2 \ll 1$. In particular, this is true for the relative signs of the direct transfer integrals $\langle \phi_{3d}^i | H_0 | \phi_{3d}^j \rangle$ and the ligand correction $\langle \chi_i | \chi_j \rangle \lambda_\pi^2 \Delta E$ (ΔE is the gap between the oxygen $2p$ band and the metal $3d$ band) since they depend only on the geometrical arrangement of the lattice. Only the relative magnitude of the two contributions change from one compound to another. In the case of Ti_2O_3 there is only one potentially magnetic a_{1g} electron for which the effective transfer integral ρ for pairs along the c axis of the corundum lattice is big, since the interference between direct and covalent contribution is additive. On the contrary, transfer to nearest neighbors in the basal plane (σ) is small since the above interference is destructive. For more distant neighbors, the direct transfer integral is negligible and the covalent contributions predominant, this latter being as small as σ, the transfer integral in the basal plane. All this is consistent with what is experimentally observed in Ti_2O_3 at low temperatures, which shows an insulating diamagnetic ground state. The system gains energy by forming diamagnetic pairs along the c axis since interaction of the two electrons in the bond with neighboring pairs is either small or hindered by the Coulomb repulsion. Hence a diamagnetic full a_{1g} bonding band is split off the upper e_g conduction band leading to an insulating state. The smooth transition observed at around 500 °K is then explained on the basis that the excitation of these bonding electrons to the upper conducting band and the consequent creation of broken pairs reduces by screening the Coulomb repulsion and tends to reduce the energy gap through a modification of the c/a ratio and a consequent increase of the jumping possibilities. Finally, the a_{1g} bonding band merging into the e_g band gives rise to a conducting state. There is no change of symmetry during this process so that the transition can be a smooth one. Cr_2O_3, on the other hand, is an antiferromagnetic insulator. This is in keeping with the fact that one expects an increasing localization of the $3d$ atomic wave functions as one moves along the first row of the transition metal series. As a result, both $\langle \phi_{3d}^i | H_0 | \phi_{3d}^j \rangle$ and $\lambda_\pi^2 \cdot \Delta E$ are smaller here than in the isostructural compound Ti_2O_3 and V_2O_3, compared to the on site Coulomb repulsion U and U'. Therefore one can apply perturbation theory of the kind used in I in order to study the most stable magnetic structure. This latter consists of ferromagnetic planes perpendicular to the c axis stacked antiferromagnetically. Again, the peculiarity of the interference between direct and covalent contribution to the effective transfer integrals explains this structure. There are three $3d$ electrons in the t_{2g} subband which are coupled to a spin-$\frac{3}{2}$ state by intra-atomic exchange (Hund's rule coupling) and the band is half full. Neglecting transfer to the higher empty E_g band (which would form weak ferromagnetic coupling along all directions) the kinetic exchange mechanism would lead to an antiferromagnetic coupling of a site to all its nearest neighbors. However, only transfer integrals along the c axis are strong enough to stabilize the antiferromagnetic coupling. The transfer integrals along the basal plane towards the three neighbors are relatively small due to the covalence destructive interference and an antiferromagnetic coupling with the much more numerous neighbors (nine) in the adjacent planes, though a moderate purely covalent exchange is preferred. Hence the experimentally observed structure is obtained.

The properties of V_2O_3 are in a series intermediate between that of Ti_2O_3 and Cr_2O_3. As extensively discussed in the previous sections, one of the two potentially magnetic electrons goes into a diamagnetic bonding band of a_{1g} character just as in the case of Ti_2O_3. The other electron goes into the doubly degenerate e_g band; however, the ratio of the on-site Coulomb repulsion energy U' to the bare e_g bandwidth is just enough to localize it at low temperature. The resulting magnetic structure is in a sense peculiar in the corundum compounds, due to the exceptional situation of the bare band being one quarter full. Since in practice there is only one e_g magnetic electron per site, the gain in intra-atomic exchange energy obtained by fully polarizing the a_{1g} electron is not sufficient to outweight the increase in kinetic energy due to localization. Hence only those a_{1g} electrons near the Fermi level become polarized and, consequently, localized. It is not until another magnetic electron is present and the bare bandwidth shrinks due to the better atomic localization of the metal electrons that we get more or less complete localization of all the potentially magnetic electrons, as is observed in Cr_2O_3 with an effective magnetic moment per site very near to 3 μ_B. This comparison serves also to illustrate the behavior of V_2O_3 doped with Ti on Cr; however, we shall not discuss here this subject which will be taken up in III.

APPENDIX

Gutzwiller's idea for constructing the ground-state wave function for a Hubbard Hamiltonian was to minimize the amplitude of all the components of an uncorrelated Bloch state in which ν atoms are doubly occupied by an amount η^{ν} with $0<\eta<1$.

Expressing the Hubbard Hamiltonian in terms of η and ν he was able to express η in terms of a $\bar{\nu}=\langle n_{1\uparrow}n_{1\downarrow}\rangle$ which minimizes the inner energy. Gutzwiller used this calculation for establishing a criterium for ferromagnetism. It was realized consequently by Brinkman and Rice[16] that $\bar{\nu}$ and g (the discontinuity in the single-particle occupation number) could be expressed in terms of the Hubbard U which gave them the following relations.

$$\bar{\nu}=\tfrac{1}{4}(1-U/U_0)\,,$$

$$g=1-(U/U_0)^2\,,$$

from which one observes the occurance of a metal to insulator transition for a critical Hubbard U_0. The effects of this highly correlated Gutzwiller's ground state onto the enhancement in the susceptibility and specific heat were noticed to be characteristically different from the enhancement factors due to paramagnons.

In order to see whether the Gutzwiller-Brinkman-Rice idea of a highly correlated electron gas can apply to V_2O_3, we have evaluated the critical values for U, U', and J for the Gutzwillers ground-state for a doubly-degenerate band Hubbard Hamiltonian. Following the work of Chao[15] and Chao and Gutzwiller[15] we find, starting from the corresponding Hubbard Hamiltonian in the Hartree-Fock approximation

$$H=\sum_{\vec{k}m\sigma}\epsilon_m(\vec{k})n_{\vec{k}m\sigma}+C_1\sum_{im\sigma}n_{im\sigma}n_{im-\sigma}$$

$$+C_2\sum_{im\neq m'\sigma}n_{im\sigma}n_{im'-\sigma}+C_3\sum_{imm'\sigma}n_{im\sigma}n_{im'\sigma}\qquad\text{(A1)}$$

that for the paramagnetic state

$$\langle H\rangle_p=g_p N\bar{\epsilon}_p+2C_1\nu_1+2C_2\nu_2+2C_3\nu_3\qquad\text{(A2)}$$

where the definition of $\nu_i\,(i=1,2,3)$ follows straightforwardly from (A.1) and

$$g_p=\tfrac{16}{3}(\tfrac{1}{4}-\nu_1-\nu_2-\nu_3)$$

$$\times[\sqrt{2}(\nu_1+\nu_2+\nu_3)^{1/2}+\nu_1^{1/2}+\nu_2^{1/2}+\nu_3^{1/2}]^2\qquad\text{(A3)}$$

$\bar{\epsilon}_p$ denotes the average band energy of the filled part of the band

$$\int_{\epsilon_{\min}}^{\epsilon_F}d\epsilon(\epsilon-\epsilon_0)\rho(\epsilon)=\bar{\epsilon}_p$$

with the normalization condition

$$\int_{\epsilon_{\min}}^{\epsilon_{\max}}d\epsilon(\epsilon-\epsilon_0)\rho(\epsilon)=0\,.$$

Minimizing $\langle H\rangle_p$ with respect to ν_i $(i=1,2,3)$, the relations

$$\frac{\partial g_p}{\partial\nu_i}=-\frac{2C_i}{\epsilon_p}\qquad\text{(A4)}$$

can be written in the form

$$\tfrac{16}{3}[\sqrt{2}(\nu_1+\nu_2+\nu_3)^{1/2}+\sqrt{\nu_1}+\sqrt{\nu_2}+\sqrt{\nu_3}]$$

$$\times\{-[\sqrt{2}(\nu_1+\nu_2+\nu_3)^{1/2}+\sqrt{\nu_1}+\sqrt{\nu_2}+\sqrt{\nu_3}]$$

$$+(\tfrac{1}{4}-\nu_1-\nu_2-\nu_3)[\sqrt{2}/(\nu_1+\nu_2+\nu_3)^{1/2}+1/\sqrt{\nu_i}]\}$$

$$=-2C_i/\bar{\epsilon}_p\,.\qquad\text{(A5)}$$

Solution of the set of Eq. (A5) provides us with the critical values U_i^0 for which the system becomes insulating. In investigating these solutions we have however to take into consideration the relation, equivalent to ours $U=U'+2J$.

$$C_1-3C_2=-2C_3$$

which leads to the equation

$$\frac{1}{\sqrt{\nu_1}}=\frac{3}{\sqrt{\nu_2}}-\frac{2}{\sqrt{\nu_3}}\,.\qquad\text{(A6)}$$

Relation (A6) indicates that ν_1, ν_2, and ν_3 must at the phase transition go to zero equally fast. In the limit $\nu_i \rightarrow 0$ Eq. (A5) together with (A6) yield

$$\begin{aligned}&\tfrac{4}{3}[\sqrt{2}(1+x_2^{-2}+x_3^{-2})^{1/2}+1+x_2^{-1}+x_3^{-1}]\\&\times[\sqrt{2}(1+x_2^{-2}+x_3^{-2})^{1/2}+1]=-2C_1/\bar{\epsilon}_p\,,\\&\tfrac{4}{3}[\sqrt{2}(1+x_2^{-2}+x_3^{-2})^{1/2}+1+x_2^{-1}+x_3^{-1}]\\&\times[\sqrt{2}(1+x_2^{-2}+x_3^{-2})^{1/2}+x_2]=-2C_2/\bar{\epsilon}_p\,,\end{aligned}\tag{A7}$$

with $x_2=(\nu_1/\nu_2)^{1/2}$ and $x_3=(\nu_1/\nu_3)^{1/2}$.

Substituting $x_3=\frac{1}{2}(3x_2-1)$ into (A7) we can easily determine the critical values C_1^0 and C_2^0 as function of any value for x_2. These solutions are plotted in Fig. (11) below. On the same figure we have also indicated the values for $C_i/\bar{\epsilon}_p$ $(i=1,2,3)$ which served as the parameters for our Hartree-Fock calculation reported in detail in this paper and for which a gap could be found. As apparent from Fig. (11) these values lie considerably below the critical values needed for the Brinkman-Rice mechanism to work. We have determined the location of these points in Fig. (11) by satisfying the relations $C_1/C_3=U/(U'-J)$ and $C_2/C_3=U'/(U'-J)$.

We should finally mention that some solutions of Eq. (A5) given by Chao and Gutzwiller which lead to lower critical values than the ones which we have determined here, are not compatible with condition $C_1-3C_2=-2C_3$.

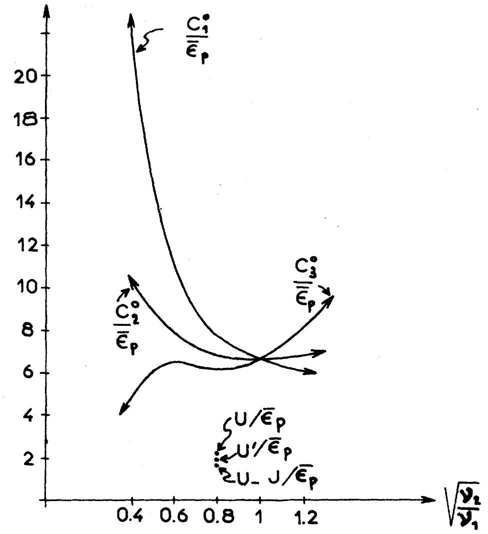

FIG. 11. Variation of the critical values $C_1=U$, $C_2=U'$, $C_3=U'-J$, the intrasite Hubbard electron-electron e_g interactions, as functions of the ratio of doubly occupied states $\nu_1/\nu_2=\langle n_1(2)_0 n_1(2)_{-\sigma}\rangle/\langle n_1(2)_\sigma n_2(1)_{-\sigma}\rangle$ according to Gutzwiller and Chao (Ref. 15). The three separate points indicated correspond to the critical values which we found by means of our unrestricted HF calculations. $\bar{\epsilon}_p$ denotes the average band energy of the filled part of the band.

---

[*] Istituto di Fisica, Università di Roma, Piazzale delle Scienze, 00100 Rome, and Gruppo Nazionale di Struttura della Materia L'Aquila, Italy.

[†] Present address: Laboratori Nazionali Frascati, Istituto Nazionale di Fisica Nucleare, 00044 Frascati, Italy.

[1] C. Castellani, C. R. Natoli, and J. Ranninger, preceding paper, Rev. B 18, 4945 (1978).

[2] P. W. Anderson, Phys. Rev. 115, 2 (1959); and *Solid State Physics*, edited by T. Seitz and D. Turnbull (Academic, New York, 1963), Vol. 14.

[3] A. C. Gossard and J. P. Remeika, Solid State Commun. 15, 609 (1974).

[4] J. M. Honig, L. L. Van Zandt, R. D. Board, and H. E. Weaver, Phys. Rev. 6, 1323 (1972); D. W. Fisher, J. Appl. Phys. 41, 3561 (1970).

[5] J. Ashkenazi and T. Chuchem, Philos. Mag. 32, 763 (1975).

[6] M. Weger, Philos. Mag. 24, 1095 (1971).

[7] J. Ashkenazi and M. Weger, Adv. Phys. 73, 207 (1973).

[8] E. Lieb and F. Wu, Phys. Rev. Lett. 20, 1445 (1968).

[9] W. Langer, M. Plischke, and D. Mattis, Phys. Rev. Lett. 23, 1448 (1969).

[10] L. M. Falikov and R. A. Harris, J. Chem. Phys. 51, 3153 (1969).

[11] S. Sugano and R. G. Shulman, Phys. Rev. 130, 517 (1963).

[12] L. F. Mattheiss, Phys. Rev. B 2, 3918 (1970).

[13] J. C. Slater and G. F. Koster, Phys. Rev. 94, 1498 (1959).

[14] L. P. Kadanoff and G. Baym, *Quantum Statistical Mechanics* (Benjamin, New York, 1962).

[15] K. A. Chao and M. Gutzwiller, J. Appl. Phys. 42, 1420 (1971); K. A. Chao, Phys. Rev. B 4, 4034 (1971); M. A. Gutzwiller, Phys. Rev. 137, A1726 (1965).

[16] W. F. Brinkman and T. M. Rice, Phys. Rev. B 2, 4302 (1970).

[17] D. B. McWhan *et al.*, Phys. Rev. B 7, 3079 (1973).

[18] J. Hubbard, Proc. R. Soc. A 281, 401 (1964).

[19] C. Castellani, C.R. Natoli, and J. Ranninger, following paper, Phys. Rev. B 18, 5001 (1978).

[20] C. Castellani, C. R. Natoli, and J. Ranninger, J. Phys. (Paris) 4, 199 (1976).

[21] J. Hubbard and W. Marshall, Proc. Phys. Soc. 86, 561 (1965); J. Owen and H. M. Thornley, Rep. Progress Phys. 29, 675 (1966); Bruce C. Tofield, *Structure and Bonding* (Springer-Verlag, Berlin, 1975).

[22] E. Simanik and Z. Sronbeck, *Electron Paramagnetic Resonance*, edited by S. Geschwind (Plenum, New York, 1972), Chap. 8, p. 543.

[23] P. Freund, J. Owen, and B. F. Hann, J. Phys. C 6, L139 (1973).